Universiteit Utrecht

Outer core structures for explaining complexity in PKP traveltime data: a Polar Caps- and Tangent Cylinder model

Madelon Smink

3872424

July, 2016

MASTER THESIS

Geophysics, Seismology Department

Utrecht University

Supervisor 1: Arwen Deuss

Supervisor 2: Hanneke Paulssen

Abstract

It has been known for a long time that, when calculating differential times, we find that polar PKPdf waves arrive sooner than predicted compared to equatorial PKPdf waves, while polar PKPbc waves arrive at similar times as predicted times. Inner core anisotropy is the general accepted explanation for this observation (Morelli et al. (1986)), but alternative models might be possible. Here we test alternative models, proposed by Romanowicz and Bréger (2000) for explaining these data: 'polar caps model' and a 'tangent cylinder model', present in the liquid outer core. The ultimate data for this research are PKPab-PKPdf and PKPbc-PKPdf differential times. The goal of this thesis is to determine whether the observations in the PKPbc-PKPdf and PKPab-PKPdf real data can be explained by waves passing through a faster velocity region inside the outer core in the form of a tangent cylinder or polar caps, without the need for inner core anisotropy. This has been done by writing Fortran programs for determining the depths where the waves enter and leave the distinct regions and use TauP for the arrival times and time spend in these regions. For the real PKPbc-PKPdf data an "L-shape" feature is observed when the residual times are plotted as a function of the angle of the ray paths with the Earth's rotation axis (ζ) and a "curve" feature for the PKPab-PKPdf dataset. The misfit and variances between the real data and cap or cylinder differential times are determined for every model. It becomes clear that for the PKPbc dataset the L-shape is indeed observed for the tangent cylinder model and a curve structure is visible for the cylinder times of the PKPab dataset with almost the same pattern as the real PKPab differential times, indicating a well fit of the tangent cylinder model with the real data. The velocities in the tangent cylinder are ±1-2% higher than in the surrounding outer core. This is in accordance with the findings of Romanowicz et al. (2003). The polar caps models show high misfits with the real data and is therefore an unrealistic model. The polar cap theory does not need to be pursued further. Even though the misfits of the tangent cylinder models with the real data are relatively low, inner core anisotropy has a lower misfit and is therefore a better fit. Still, the tangent cylinder model cannot be excluded from considerations, since the misfit with the data is low and the velocity increase within the tangent cylinder are possible. The sustainability of heterogeneities within the liquid outer core, however, is still in question.

Another question is the presence of the hemispheres within the core. In this study, no hemisphere are included in the outer more models, still, differences in cap and cylinder times between the eastern and western hemisphere are observed. Therefore the paths are such that it seems like there are hemispheres in the core, and we should be careful with the interpretation of the inner core having hemispherical differences.

Contents

Chapter 1

Introduction

The Earth's fluid outer core was first discovered by Oldham (1906) and it was the seismologist Lehmann (1936) who suggested that the Earth has a solid inner core. She observed that seismic waves reflect off the boundary of the inner core. The liquid outer core plays a significant part in global Earth dynamics, rotation, the chemical differentiation and the generation of the magnetic field (Souriau and Poupinet (1990)). The outer core is generally believed to be homogeneous due to convection and its inability to sustain density heterogeneities (Stevenson (1987)).

Solidification of the inner core supplies some of the heat that drives mantle convection and therefore plate tectonics at Earth's surface. The core is therefore very important for understanding the working of the Earth. It is seismically observed that the propagation times of compressional body waves that travel the inner core are faster for wave directions quasi- parallel to the Earth's rotation axis than equatorial-directed waves. This observation was first discovered by Poupinet et al. (1983). Subsequently, Morelli et al. (1986) proposed inner core anisotropy to explain these body wave observations (short period). Furthermore, inner core anisotropy also explained the normal mode (long period) observations (Woodhouse et al. (1986)). In multiple studies, these observations for as well the body waves as the core modes were confirmed (Su and Dziewonski (1995); Shearer et al. (1988); Ritzwoller et al. (1986)).

It was found that the top ~100 km of the inner core may be isotropic, since the PKIKP-PKiKP body waves, which are sensitive to the upper 100 km of the inner core, show little anisotropy. Waves that travel more than 60 km below the inner core boundary show a small amount of anisotropy, suggesting that the isotropic layer will be limited till 50 - 80 km thick and varies laterally (Song and Helmberger (1998)).

For the first inner core anisotropy models, transverse isotropy with the fast axis parallel to the Earth's rotation axis was proposed. This is expected if the anisotropy were due to the alignment of hcp-iron crystals with the axis of rotation (Stixrude and Cohen (1995)). However, the data have expanded over the years and more details about the inner core's structure have been published. It was proposed that the symmetry axis of inner core anisotropy was tilted with respect to the Earth's rotation axis to explain the variations of polar wave arrival times with varying turning longitude in the inner core (Su and Dziewonski (1995)). More recently, Tanaka and Hamaguchi (1997) showed that an asymmetry was present in the inner core in terms of two hemispheres. The western hemisphere is more strongly anisotropic and has

a lower isotropic velocity than the eastern hemisphere (Tanaka and Hamaguchi (1997)). The need for a tilted anisotropy axis was no longer necessary, the inner core shows lateral variations instead. The hemispherical variations are not only the best fit for the body wave observations but also for normal mode observations (Deuss et al. (2010)). Some studies propose that an innermost inner core is present, where at a radius of 400 km the polar directed waves are slow and the equatorial directed waves fast (Beghein and Trampert (2003); Ishii and Dziewoński (2002)). However, the evidence for an innermost inner core is not compelling (Deuss (2014)).

Other models have been suggested to explain the observations, instead of inner core anisotropy; Bréger et al. (1999) suggested that the observed faster polar directed-waves and the slower equatorial-directed waves can also, for a significant part, be explained by strong heterogeneity in D"-layer at the base of the mantle, and Bréger et al. (2000) suggested a possible combination of the D" structure and inner core anisotropy to explain the data. Furthermore, an interpretation for deviating mode splitting, proposed by Ritzwoller et al. (1986), is by outer core heterogeneity.

According to Romanowicz et al. (2003), hemispherical inner core anisotropy models fail to reproduce the characteristic "L-shape" of PKP body wave travel time residuals when they are plotted as a function of the angle with respect to the Earth's rotation axis (chapter 4).

Due to the complexity of inner core anisotropy models and the influence of strong heterogeneity at the base of the mantle for explaining the data, it is important to consider whether the observed fast waves in the direction parallel to the rotation axis, originates in the inner core, outer core, or mantle.

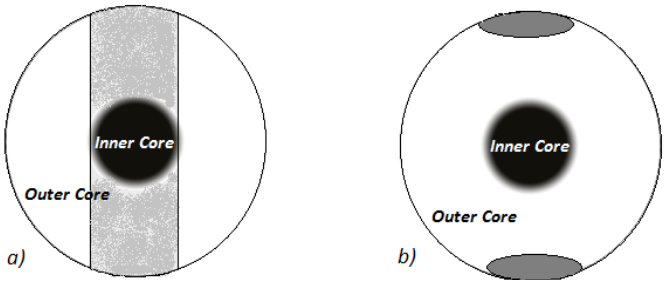

Figure 1.1: *Core research models: a) tangent cylinder and b) polar caps in outer core*

An alternative model is proposed by Romanowicz and Bréger (2000), they showed that most of the C20 mode anomalies are fully explained by heterogeneities in the liquid outer core, without the need for inner core anisotropy. The observations are, according to Romanowicz and Bréger (2000), explainable by either P-velocity and density perturbations inside the tangent cylinder in the direction of the Earth's rotation axis (figure 1.1a), or the presence of two polar caps (figure 1.1b) (Romanowicz and Bréger (2000)). The tangent cylinder model, with 1% faster velocity inside the tangent cylinder, is preferred by Romanowicz et al. (2003), since the tangent cylinder model can reproduce the "L-shape" feature of the PKP body wave travel time data.

In this study, we will investigate the "polar cap" model and "tangent cylinder" model in the liquid outer core, proposed by Romanowicz and Bréger (2000); Romanowicz et al. (2003), for trying to explain observations of short period body wave data which travel the inner core. In figure 1.1 both alternative core models are shown. Short period PKP body waves are the ultimate data to test if the tangent cylinder or polar caps in the outer core need to be considered or if inner core anisotropy remains the best explanation for the anomalous body wave observations.

Chapter 2

Methods

As stated before, mostly inner core anisotropy and some alternative hypotheses are used for explaining the faster polar directed waves and slower equatorial directed waves. To check for outer core structure we use bodywaves that pass through both the outer core and through the inner core. We use in this study PKPdf (same term as 'PKIKP') waves, PKPab and PKPbc waves (figure 2.1). The PKPdf wave has its turning point inside the inner core, therefore it travels through the mantle, liquid outer core and the inner core. The PKPbc and PKPab waves are the reference phases and travel through the mantle and the liquid outer core, where they have their turning point (figure 2.1).

The PKPbc wave has a similar path as the PKPdf wave, only the turning point of the PKPdf wave is in the inner core and the PKPbc wave turning point in the outer core. The PKPab wave has a more deviating path from the PKPdf wave than the PKPbc wave, therefore crust- and mantle structure corrections have to be made. The PKPab wave has a turning depth closer near the core-mantle boundary than the PKPbc wave (figure 2.1).

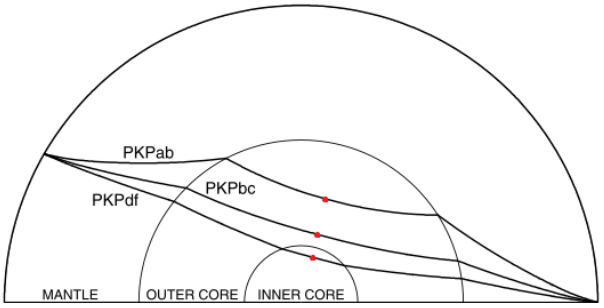

Figure 2.1: *Bodywave paths used for this study: PKPdf, PKPbc and PKPab waves, the red dots indicate the turning points of the waves.*
(*Irving and Deuss (2011)*)

We are interested in studying the variation of travel time with the angle ζ between the ray path and Earth's rotation axis. Waves with an angle exceeding ζ>35° with respect to the Earth's rotation axis, are 'equatorial waves' and waves with an angle lower than ζ<35° with respect to the Earth's rotation axis, are called 'polar waves' (figure 2.2). We use both waves to check if the polar waves are faster than the equatorial waves in our data. Alternatively, for the polar caps and tangent cylinder hypotheses, the velocity of these waves depends on whether the waves cross the polar caps or tangent cylinder or not. The ζ is not important for these models.

We use the travel times of the real data and the travel times of the model AK135 (Kennett et al. (1995)) to calculate the differential times (δt):

$$\delta t = (t_{PKPbc/ab} - t_{PKPdf})_{meas(data)} - (t_{PKPbc/ab} - t_{PKPdf})_{pred(AK135)} \quad (2.1)$$

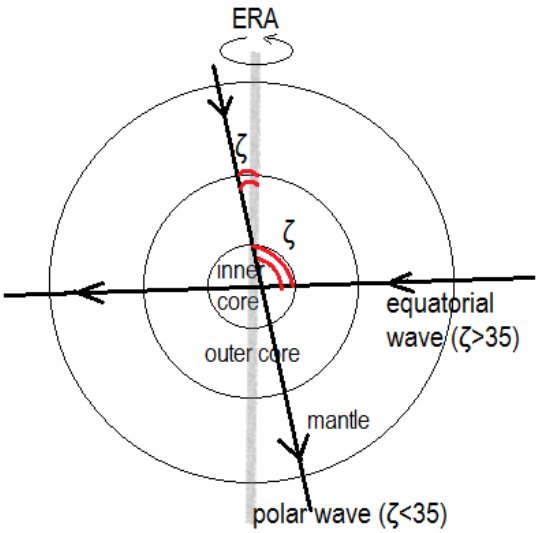

Figure 2.2: *The angle of the incoming PKIKP waves with the Earth's rotation axis (ERA) is indicated as ζ. If ζ>35° the waves are equatorial and if ζ < 35° the waves are called 'polar waves'.*

Here, δt is the differential time of the real data, t_{PKPdf} is the travel time of the PKPdf wave and $t_{PKPbc/ab}$ is the travel time of the PKPbc or PKPab wave. By taking the differential travel times we remove the influence of the crust and the mantle. The equation shows that for polar waves, when the PKPdf waves arrive earlier than predicted by the AK135 model (Kennett et al. (1995)), the δt value increases. For equatorial waves the PKPdf arrival times measured are similar to the predicted arrival times and therefore the δt value is near zero.

To get information about e.g. the paths of the waves within the Earth, we use the seismic travel time calculator, TauP. With this program we calculate the travel times of PKPdf, PKPbc and PKPab waves for different pierce points in the Earth. We use TauP_path to get for every radius in the Earth the latitude and longitude per wave. With the generated output files (appendix D) we can establish if the waves pass through the polar caps and tangent cylinder or not. To determine the depths when the various waves enter and leave the tangent cylinder or polar caps, we wrote Fortran programs (appendix A-C).

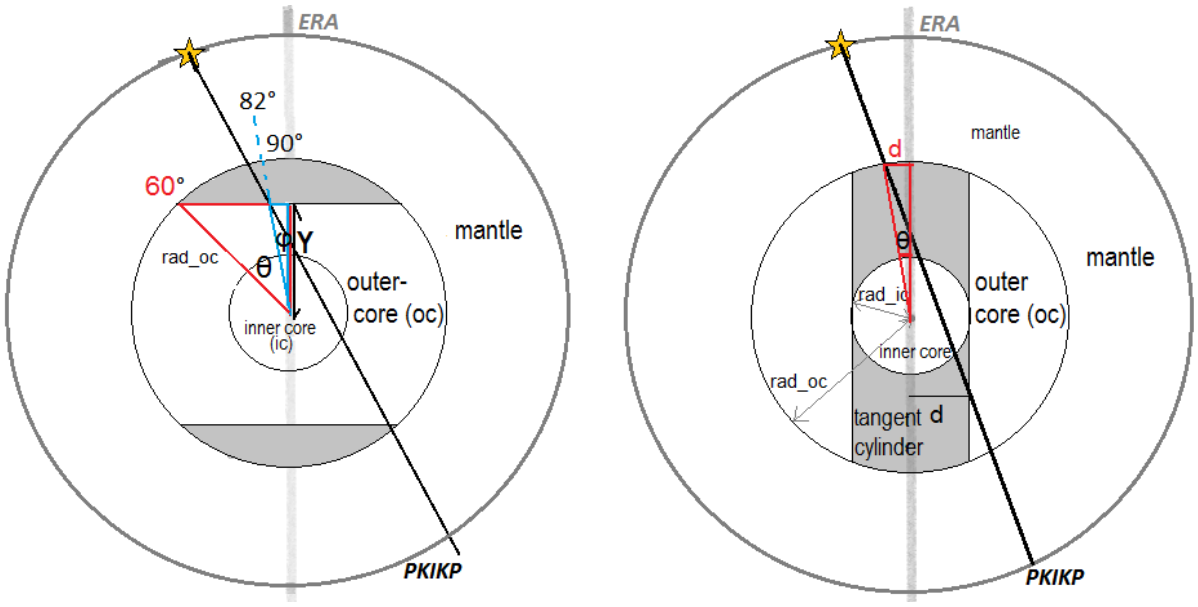

(a) (b)

Figure 2.3: *This figure shows the Fortran program method in a schematic way for determining the in- and out depths of the a) polar caps model and b) tangent cylinder model. a) θ is the angle between the latitude of the cap boundary (here 60°) and the top latitude (90°) therefore θ=30°. φ is the angle between the latitude of the wave when leaving the polar cap (here 82°) and the top latitude (90°), therefore φ=8°. b) d is the absolute distance between the rotation axis and the wave. d can be calculated using the red triangle by use of the angle between the latitude of the ray and the maximum latitude, indicated as θ. These figures are only shown for PKIKP waves, but the same method is applied for the PKPbc and PKPab waves (appendices A-C). rad_oc is the radius of the outer core and rad_ic is the radius of the inner core. The yellow star indicates the Earthquake.*

This is done, for the polar cap models, by using the angles (φ) between the ray paths and the maximum latitude (90°) and the angle (θ) between the maximum polar latitude (90°) and the boundary latitude of the polar caps (e.g. 60°), shown in figure 2.3a. With the red triangle, where the θ value and radius of the outer core are known, the distance Y can be determined for every cap thickness depending on the cap boundary latitude. In figure 2.3a θ=30°. Thereafter with the blue triangle, in figure 2.3a, with the known Y length and the known angle φ between maximum latitude and latitude of the wave when leaving the cap using TauP, the hypotenuse (the radius to the leaving point of the ray) can be determined. This is the depth we want to know for determining the travel time of the wave at this point.

For the tangent cylinder, we look at the distance between the Earth's rotation axis and the ray path, indicated in figure 2.3b. If the distance, from the outer core boundary, is smaller than the inner core radius, the wave is inside the tangent cylinder. The distance d can be calculated with radius of the wave at any point in the Earth, multiplied by the sine of the corresponding angle θ (90-latitude, red triangle in figure 2.3b). Therefore for every radius and corresponding latitude, the distance is calculated by the program and when the distance is smaller than the inner core radius, the wave is inside the tangent cylinder (appendix B and figure 2.3).

If we have determined the depths at which the waves enter and leave the tangent cylinder or polar caps, the in- and out-times of the waves at these depths can then be calculated by TauP_pierce.

The time difference between the PKPdf - PKPbc/PKPab that the waves spend in the polar caps or tangent cylinder ($t_{cap/cyl}$), is linearly related to the differential times of the measured data (δt_{meas}).

The following equation shows this relation:

$$\delta t_{meas} = A_{cyl} \times t_{cyl} \tag{2.2}$$

$$\delta t_{meas} = A_{cap} \times t_{cap} \tag{2.3}$$

Where $A_{cap/cyl}$ is the model parameter. For inner core anisotropy it is not a linear relation, but a cosinus-relation (Creager (1999)). Assuming cylindrical anisotropy with Earth's rotation axis as symmetry axis, the body wave travel time measurements are modelled following Creager (1999):

$$\frac{\delta t_{anisotropoy}}{t_{ic}} = A + B \cdot \cos^2(\zeta) + C \cdot \cos^4(\zeta) \tag{2.4}$$

Where δt is the travel time perturbation and t_{ic} the travel time of the wave in the inner core. Between purely polar (ζ=0) and purely equatorial (ζ=90) waves the B + C quantifies the amount of anisotropy defined as the difference in travel time residual (equation 2.4). A is indicated as the perturbation in equatorial velocity.

$$\delta t_{anisotropy} = (A + B \cdot \cos^2(\zeta) + C \cdot \cos^4(\zeta)) \cdot t_{ic} \tag{2.5}$$

We determine the average model parameters A_{cap}, A_{cyl}, A, B and C by fitting the real data with the models using the equations above. The $A_{cap/cyl}$ values, for each datapoint, are summed and divided by the number of datapoints to get the average: $\overline{A}_{cap/cyl}$. The determined differential times per model are now calculated with the average model parameters with the following equations:

$$\delta t_{cyl} = \overline{A}_{cyl} \times t_{cyl} \tag{2.6}$$

$$\delta t_{cap} = \overline{A}_{cap} \times t_{cap} \tag{2.7}$$

Then, the misfit of the data with the cap, tangent cylinder and inner core anisotropy models is determined by using the following equation:

$$misfit = \frac{\sum \sqrt{(\delta t_{cap/cyl/ani} - \delta t_{meas})^2}}{N} \tag{2.8}$$

Where N is the number of datapoints and $\delta t_{cap/cyl/ani}$ are calculated in the above equations (2.5, 2.6 and 2.7). The results of all misfit values are given in chapter 4.

The polar cap model is tested for various thicknesses of the caps. These thicknesses are indicated for every latitude boundary in table 2.1.

Table 2.1: *Absolute depths cap boundaries and thicknesses of caps*

Model	Max depth cap	Absolute max depth
Cap lat 50	3712.06 km	812.06 km
Cap lat 55	3527.72 km	627.72 km
Cap lat 60	3365.03 km	465.03 km
Cap north	3365.03 km	465.03 km
Cap south	3365.03 km	465.03 km
Cap lat 65	3225.21 km	325.21 km
Cap lat 70	3109.33 km	209.33 km

Chapter 3

Data

We downloaded the data using Wilber on the IRIS webpage. The events we use in this study are from the time period 2001 - 2016, with one event from 1992, for various locations (figure 3.1). Most events, with seismic waves quasi-parallel to the earth's rotation axis, are from the South Sandwich Islands region. The equatorial waves we use, are from locations such as Colombia, Argentina, Fiji, Peru or Indonesia.

We use PKPab-PKPdf and PKPbc-PKPdf differential times, which we measure on vertical component records (BHZ) for a moment magnitude range of 5.3 - 6.2 Mb. For the PKPbc waves we use an epicentral distance range of 148 – 155° and for the PKPab waves a range of 155 – 180° (figure 3.2).

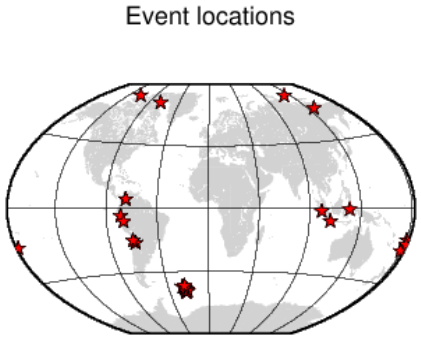

Figure 3.1: *Locations of events for both the PKPab and PKPbc dataset containing both equatorial waves and polar waves.*

The PKPab dataset consists of eighteen events and a total of 254 seismograms.The PKPbc dataset consists of thirteen events and a total of 146 seismograms (table 3.1). All earthquakes have at least a depth of 12 km. To get the correct latitude-, longitude-, depth- values and event times for the different events, we use the EHB Bulletin (Dziewonski et al. (1981), Ekström et al. (2012)) and the CMT catalog (Engdahl et al. (1998)).

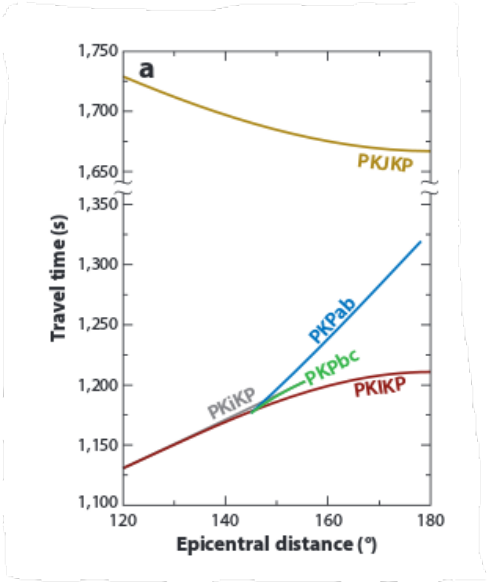

Figure 3.2: *Travel time curves with the epicentral distances of the PKIKP (PKPdf), PKPab and PKPbc phases*

(*Deuss (2014)*)

Table 3.1: *Dates, locations and number of stations of events in data sets*

Date event	Location event	lat(°)	lon(°)	depth(km)	Data set	Nr of stations
2001-04-13	south-Sandwich-islands	-59.839	-25.699	26.0	PKPbc	13
2002-02-10	south-Sandwich-islands	-55.959	-28.993	193.0	PKPbc	16
2004-09-11	south-Sandwich-islands	-58.035	-25.402	71.9	PKPbc	34
2006-05-29	south-Sandwich-islands	-59.637	-26.29	48	PKPbc	14
2007-07-31	south-Sandwich-islands	-56.101	-27.773	114.2	PKPbc	14
2016-02-18	south-Sandwich-islands	-56.28	-27.04	108.9	PKPbc	14
2014-09-10	southern-Molucca	-0.36	125.06	29.2	PKPbc	1
2011-10-27	Fiji Islands	-17.98	-179.4	608.7	PKPbc	3
2012-09-20	Fiji Islands	-20.64	-178.3	569.6	PKPbc	7
2013-10-24	South of Fiji	-22.73	-176.2	136.8	PKPbc	1
2014-12-14	Fiji Islands	-20.950	-176.560	254.20	PKPbc	11
2015-03-10	Northern-Columbia	6.83	-73.11	155.9	PKPbc	13
2015-09-07	South of Fiji	-24.28	179.07	551.6	PKPbc	5
2004-02-22	southern-Sumatra-Indonesia	-1.613	100.396	46.3	PKPab	16
2010-05-19	northern-Peru	-5.13	-77.55	132.2	PKPab	12
2011-04-26	Jawa-Indonesia	-8.38	108.4	81.5	PKPab	1
2012-11-10	Central-Peru	-8.88	-75.17	133.2	PKPab	26
2014-09-24	Jujuy-province-Argentina	-23.78	-66.72	227.6	PKPab	21
2015-03-10	northern-Colombia	6.83	-73.11	155.9	PKPab	9
1992-02-17	Severnaya-Zemlya-Russia	79.171	124.494	22.2	PKPab	1
2002-02-10	south-Sandwich-islands	-55.85	-28.81	199.0	PKPab	6
2004-09-11	south-Sandwich-islands	-58.13	-24.93	29.00	PKPab	7
2008-04-14	south-Sandwich-islands	-56.055	-28.089	130.0	PKPab	17
2008-10-07	Arctic-ocean	79.77	-116.02	12.0	PKPab	3
2009-07-07	Baffin-bay	75.33	-72.49	16.5	PKPab	17
2010-06-02	south-Sandwich-islands	-57.64	-26.11	135.1	PKPab	20
2010-07-12	northern-Chile	-22.4	-68.61	134.7	PKPab	58
2013-02-14	eastern-Siberia-Russia	67.65	142.51	12.0	PKPab	21
2013-03-19	south-Sandwich-islands	-59.1	-23.87	34.8	PKPab	1
2014-02-01	south-Sandwich-islands	-56.97	-26.72	131.9	PKPab	8
2016-04-19	south-Sandwich-islands	-55.64	-27.09	18.9	PKPab	10

Furthermore, we use the Seismic Analysis Code (SAC) for data recovery and phase picking in the seismograms (figure 3.3, 3.4 and 3.5). For the PKPdf-PKPbc data set we pick waves by picking the maximum or minimum in the seismograms, which is indicated in figure 3.3. This works well for the

PKPbc, since they have the same waveform as PKPdf. The PKPab, however, has a different waveform than the PKPdf, so this does not work for PKPab. This is because the PKPab wave is caustic, which means that they all first converge to a point and then diverge from that point to the station. A Hilbert transform must be applied. To pick the right arrival times, we pick the onset of the PKPab- and the PKPdf wave, where the energy starts to increase (figure 3.4 and 3.5). Outliers of the data are eliminated from the dataset and the data are corrected for ellipticity.

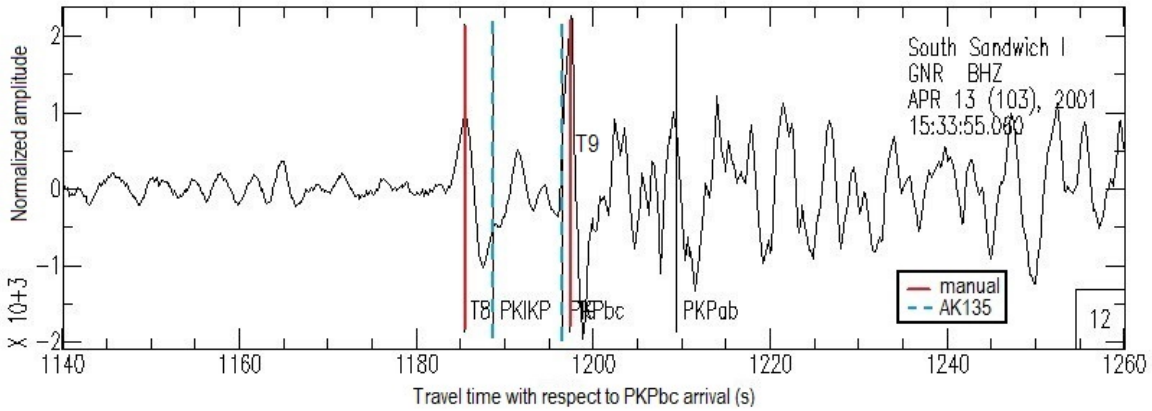

Figure 3.3: *T8 = PKPdf (PKIKP) manually picked and T9 is PKPab manually picked (red lines) and the blue dotted lines are the estimated arrival times according to the AK135 model, for a polar wave*

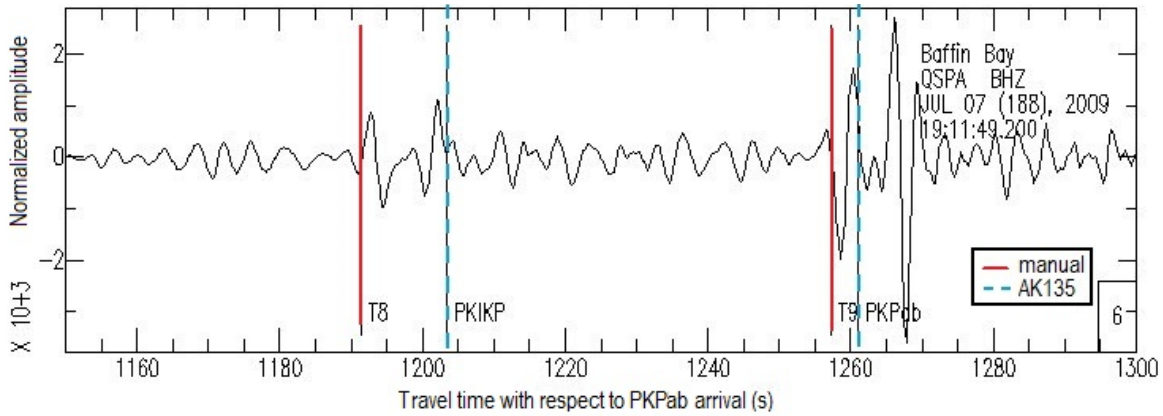

Figure 3.4: *T8 = PKPdf (PKIKP) manually picked and T9 is PKPab manually picked (red lines) and the blue dotted lines are the estimated arrival times according to the AK135 model, for a polar wave. It is also clear that for these polar waves the real data shows that the PKIKP wave arrives sooner than predicted by the AK135 model and the PKPab wave arrives at a similar time as the predicted PKPab wave by the AK135 model.*

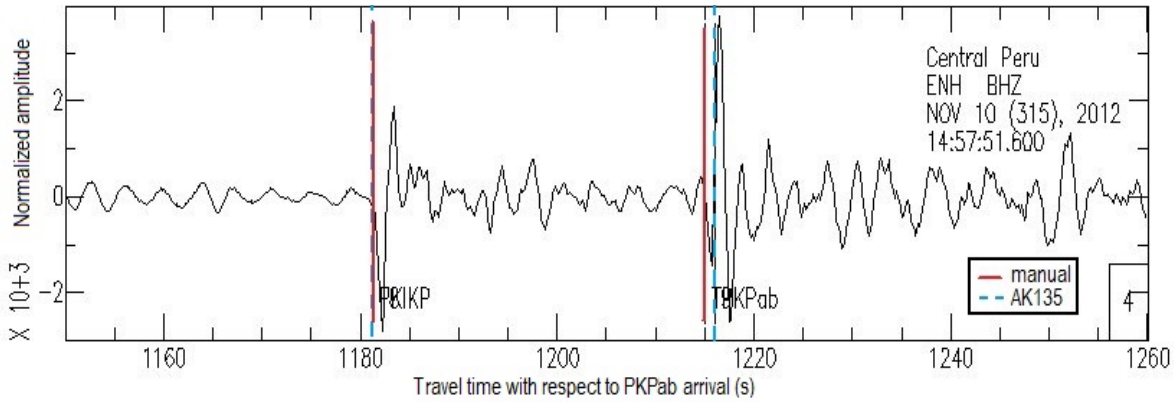

Figure 3.5: *T8 = PKPdf (PKIKP) manually picked and T9 is PKPab manually picked (red lines) and the blue dotted lines are the estimated arrival times according to the AK135 model, for an equatorial wave. It is clear that for these equatorial waves, the PKIKP and PKPab waves of the real data (red lines) arrive at similar times as the predicted arrival times by AK135 (blue dotted lines).*

Chapter 4

Results

Here, we show the results of the real data-, cap- and tangent cylinder residual times as a function of ζ for the PKPbc-PKPdf and PKPab-PKPdf datasets. The programs that we made for calculating the in- and out- depths of the waves for the tangent cylinder and polar caps are given in appendices A - C. An example of the depths and arrival times of PKIKP waves, where they enter and leave the tangent cylinder, that we have calculated using the Fortran programs in appendix A - C and TauP, is shown in appendix D. Furthermore, the model misfits and variances are shown and the corresponding velocities in caps and cylinder.

4.1 Data

The PKPab-PKPdf and PKPbc-PKPdf datasets contain both waves that have small (ζ<35°) angles with the Earth's rotation axis (polar waves) and equatorial waves, with an angle > 35° to the Earth's rotation axis. Most PKPbc-PKPdf polar paths pass the western hemisphere (longitude: -180° till 0°) and a few pass the eastern (longitude: 0°-180°) hemisphere (figures 4.1 and 4.2). The PKPbc-PKPdf equatorial paths are more spread and almost every area, besides the southwestern part, is covered. The PKPab-PKPdf dataset contains more paths and covers therefore all areas of the core for as well the equatorial paths as the polar paths (4.2). The colored triangles and circles indicate the measured differential times, which show that the polar paths in both datasets have higher differential times. The PKPbc polar waves have lower differential times in the eastern hemisphere than in the western hemisphere.

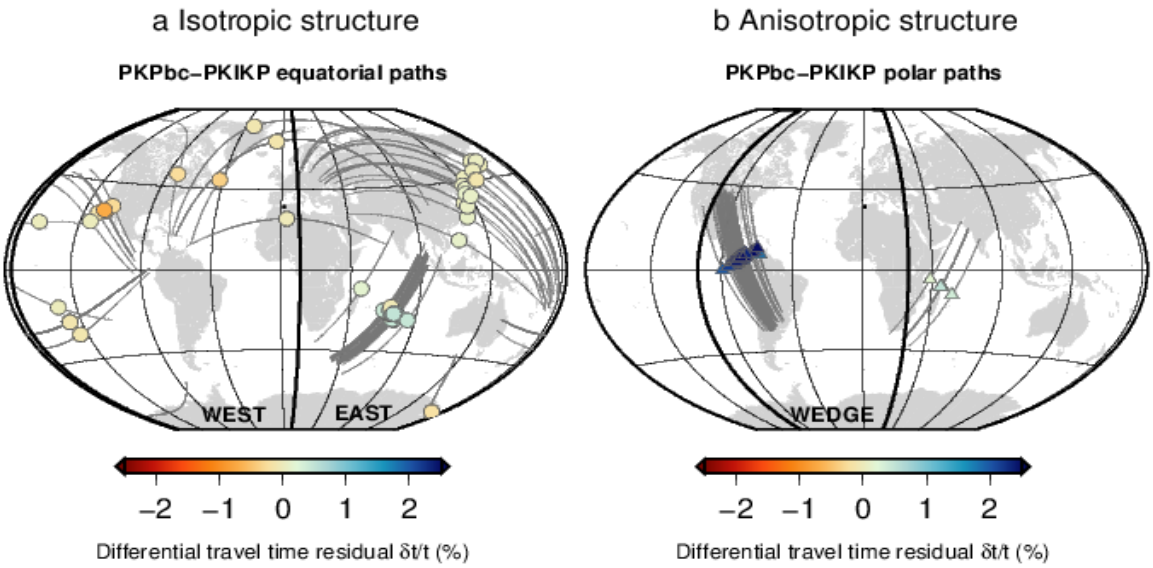

Figure 4.1: *The PKPbc-PKPdf observations of their paths inside the core are shown and their difference in equatorial paths and polar paths. For every path differential travel time residuals are indicated by the colors.*

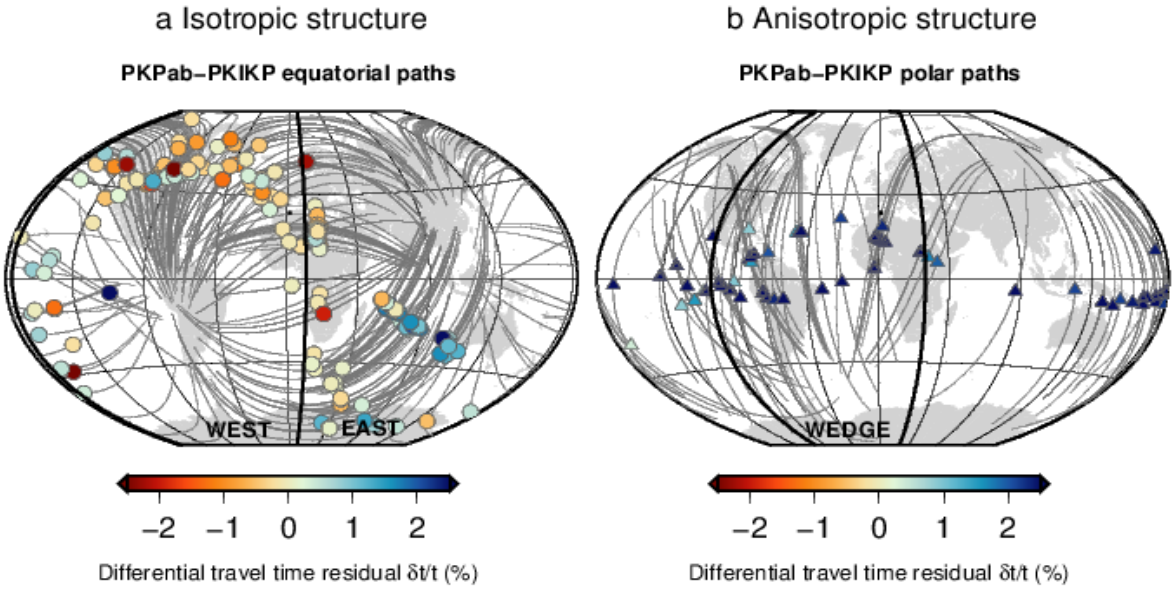

Figure 4.2: *The PKPab-PKPdf observations of their paths inside the core are shown and their difference in equatorial paths and polar paths. For every path differential travel time residuals are indicated by the colors.*

By using the differential time equation (2.1) we observe that the PKPdf (PKIKP) waves arrive sooner for polar waves in the data, compared to the PKPdf arrival times from the AK135 model, than for the equatorial waves (e.g. figure 3.4 and 3.5). We observe for $\zeta > 35°$ (e.g. seismogram in figure 3.5) that the differential times (δt) are around zero (δt=~0 sec) and a relatively sharp increase for $20 < \zeta < 35°$ occurs where the differential times are positive values ($0 < \delta t < 7$ sec). This feature is similar to an "L-shape". The "L-shape" is visible in figure 4.3. For the PKPab-PKPdf dataset (figure 4.4), we observe a similar feature: for $\zeta > 40°$ the differential times vary from -4 till 1 sec, for $35° < \zeta < 40°$ the differential times vary from -3 till 6 sec and for $5° < \zeta < 35°$ the δt varies from 0 till 10 sec. The differential times increase more smoothly when ζ decreases and it therefore gives a more "curved" trend. The "curve" feature is shown in figure 4.4. From figure 4.3 and 4.4 we notice that the PKPab-PKPdf dataset shows more scattering in the data than PKPbc-PKPdf dataset. This can be explained by that the PKPbc path is more similar to the PKPdf path than the PKPab path (figure 2.1). The data are corrected for ellipticity. We found events for the PKPab-PKPdf dataset that have wave paths with a very small angle to the Earth's rotation axis ($\zeta < 20°$), these cause scattering of polar wave data points in the PKPab-PKPdf dataset. Still the waves with a very small ζ value have relatively large differential times, as is expected (figure 4.4).

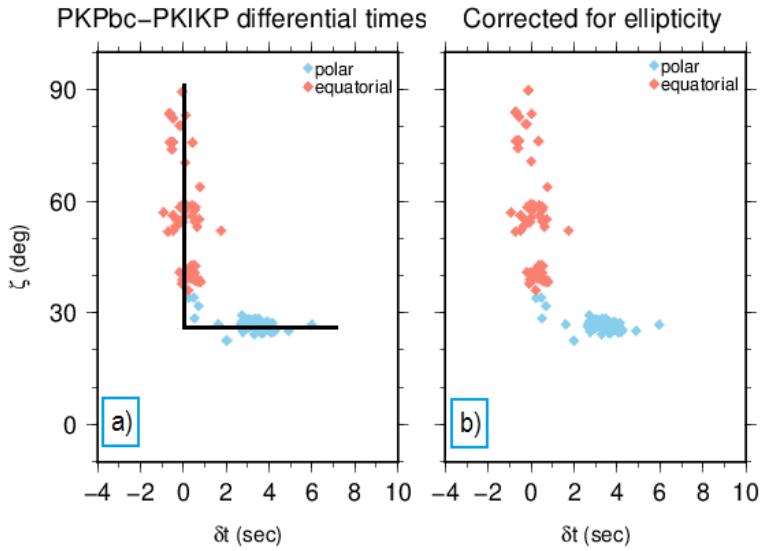

Figure 4.3: *We plotted here the real data PKPbc-PKPdf differential times versus ζ, with (b) and without (a) correction for ellipticity. An "L-shape" feature is visible in the PKPbc-PKPdf data.*

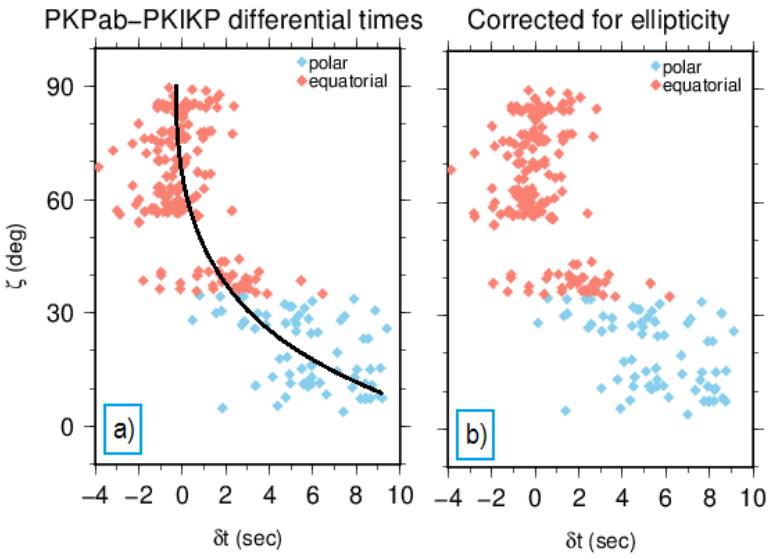

Figure 4.4: *The real data PKPab-PKPdf differential times versus ζ are plotted, with (b) and without (a) correction for ellipticity. A "curve" feature is observed for the PKPab-PKPdf dataset. The data is more scattered than PKPbc-PKPdf data.*

4.2 Polar caps

The polar caps model suggests that distinct polar cap regions are situated at the poles in the liquid outer core. To get an idea of the size of the caps, we run the programs for different cap latitudes for as well the PKPab-PKPdf waves as the PKPbc-PKPdf waves. This means that the lower boundary of the cap will vary (figure 4.5). The thicknesses of the caps are shown in table 2.1. Furthermore, to check if both caps are necessary for the best fit with the data, we run the program for the north and south polar cap separately as well. The cap times are calculated using the following equation (4.1):

$$t_{cap} = t_{cap\_PKPdf} - t_{cap\_PKPbc/ab} \tag{4.1}$$

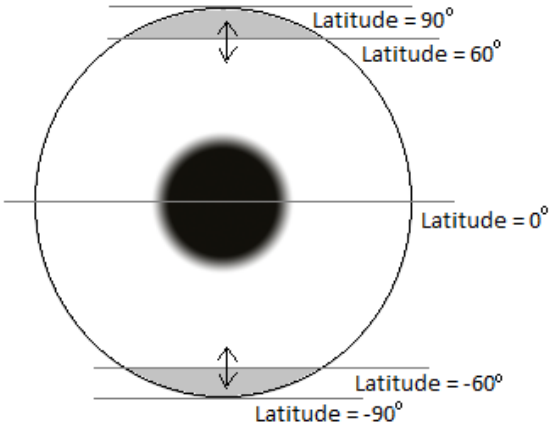

Figure 4.5: *Polar caps within the outer core, with varying lower boundary, depending on latitude. As an example, here the boundary cap latitude is 60°.*

If for polar PKPdf waves spend more time in the caps than PKPbc waves, it can explain why PKPdf waves arrive sooner than is predicted by the AK135 model. As mentioned before, the polar cap model is fitted with the real PKPbc-PKPdf/ab data by the A_{cap} parameter in equation 2.3. The average parameter $\overline{A}_{cap}$ is then multiplied by all cap differential times, which give δt_{cap} values (using equation 2.7), and plotted as a function of ζ in order to get the differential times of the models and the real data in the same order of magnitude and can be compared to each other.

4.2.1 Polar caps model for PKPbc dataset

The real data can be directly compared to figure 4.6a2, b2, c2 and 4.7a2, since here the cap differential times are multiplied by the $\overline{A}_{cap}$ parameter and therefore have the same scale as the real data, as described above (equation 2.7). It is visible that the cap model with a latitude of 50° (figure 4.6a2) fits best with the real data (figure 4.6a3) even though the cap model with a latitude of 60° (465.0. km thickness) has the most obvious "L-shape". The misfit of the models with the data is shown in table 4.2. With decreasing cap thickness (figure 4.7)a1), the "L-shape" is not visible anymore; almost no PKPdf waves spend more time in the caps than PKPbc waves (figure 4.7a). We observe, for equatorial directed waves, negative cap differential times (especially for caps with larger cap sizes) or values near zero (figure 4.6a-b). Negative cap differential times contradict the data and therefore cause higher misfits. The polar caps model with a latitude of 70° (209.33km) does not work for our dataset, since both PKPdf and PKPbc waves do not cross the caps.

For either a north or a south cap, with a latitude of 60° or -60°, the most clear "L-shape" feature is for only a north cap present in the outer core (figure 4.7b1 and b2). For only a south cap present, no PKPdf polar wave travels longer in the south cap than PKPbc polar waves, therefore this model does not fit the data well and is not being considered further. The results show that the polar cap model for the PKPbc-PKPdf dataset do not explain all data observations. The most clearly defined "L-shape", with the least scattering, is when the lower (upper) latitude boundary of the caps is 60° (-60°) and the misfit, visible in table 4.2, is lowest for a cap model with a latitude of 50° due to least differential time differences using equation 2.8.

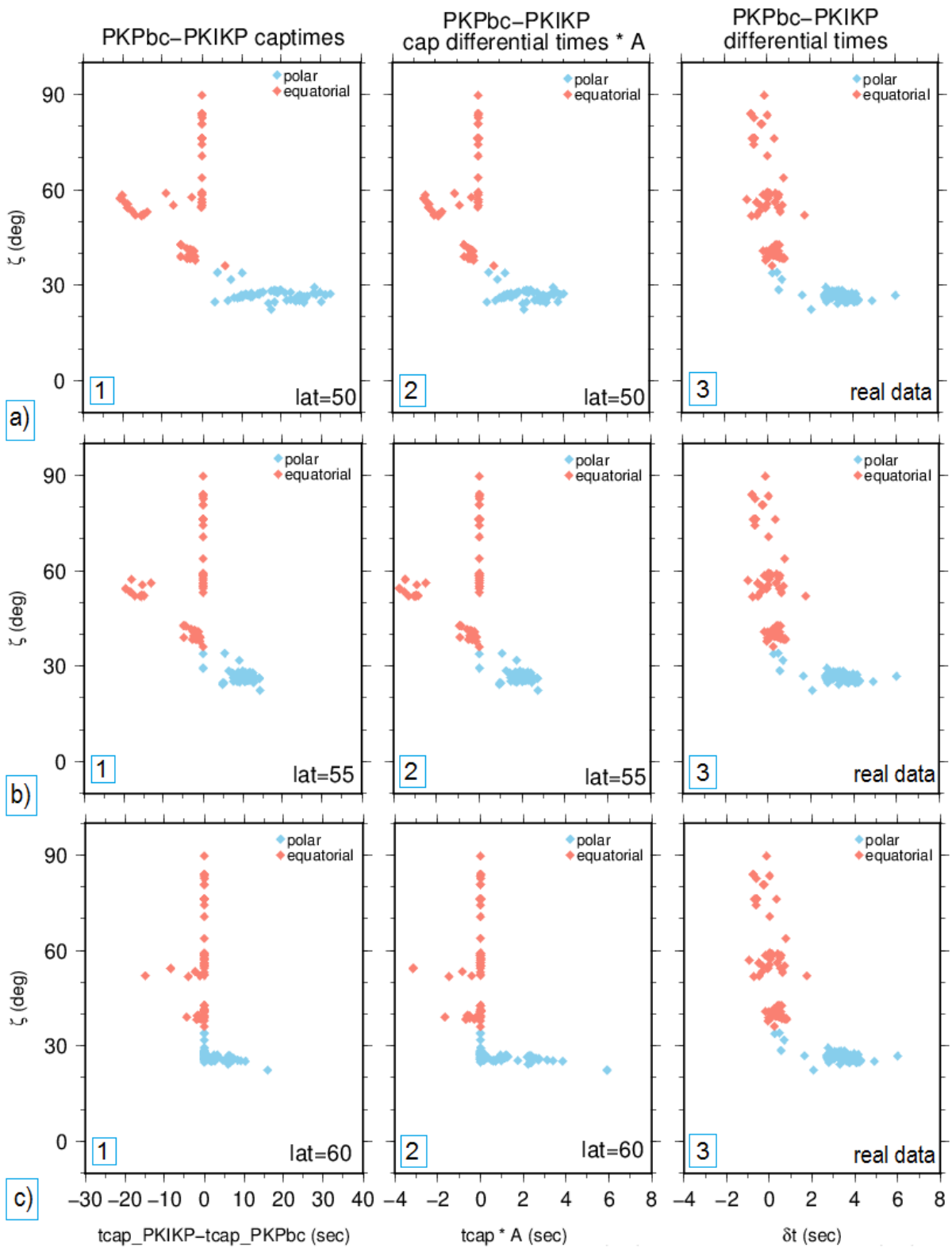

Figure 4.6: *Travel time difference between PKPbc and PKIKP for time spent in a cap with latitudes of (a) 50°, (b) 55° and (c) 60° as a function of ζ between the ray path in the inner core and Earth's rotation axis. The differential times of the real data (3), the cap differential times multiplied by the average $\overline{A}$ parameter (for $\overline{A}$ values see table 4.2) (2) and the cap differential times (1) are plotted as a function of ζ.*

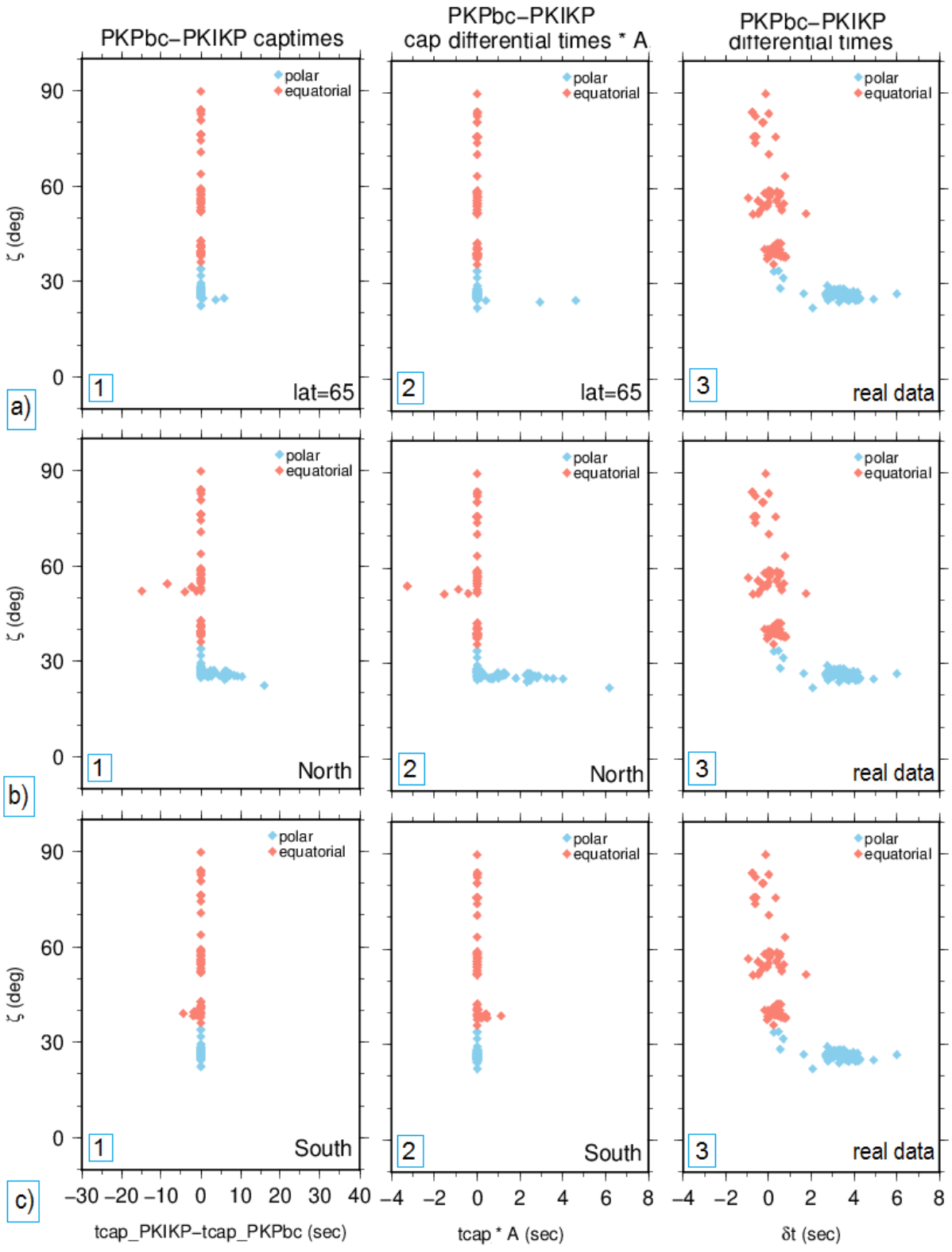

Figure 4.7: *Travel time difference between PKPbc and PKIKP for time spent in a cap with latitudes of (a) 65° and a separate (b) north cap with cap latitude of 60° and (c) south cap (cap latitude of 60°) inside the outer core as a function of ζ between the ray path in the inner core and Earth's rotation axis. The differential times of the real data (3), the cap differential times multiplied by the average $\overline{A}$ parameter (for $\overline{A}$ values see table 4.2) (2) and the cap differential times (1) are plotted as a function of ζ.*

4.2.2 Polar caps model for PKPab dataset

We next investigate PKPab-PKPdf for the same cap sizes (figures 4.8, 4.9 and 4.10). The time differences of the time spent in the caps between PKPdf (PKIKP) and PKPab waves are larger than the time differences between the PKPdf and PKPbc waves. When the thickness of the caps decrease the "curve" trend becomes less clear when ζ is plotted against cap differential times (figures 4.9a1 and b1).

All cap models show a "curve" feature when ζ is plotted against the cap differential times multiplied by $\overline{A}_{cap}$. Both the models and the real data (figure 4.4) show negative differential times for some equatorial waves and positive differential times for polar waves. There are, however, more negative cap time differences than is observed in the real data (figure 4.8c2). When the cap thicknesses decrease, the abundances of negative cap differential times decrease (figures 4.9a2 and b2). The smallest misfit for the PKPab-PKPdf dataset, is for the cap model with boundary latitude of 55°.

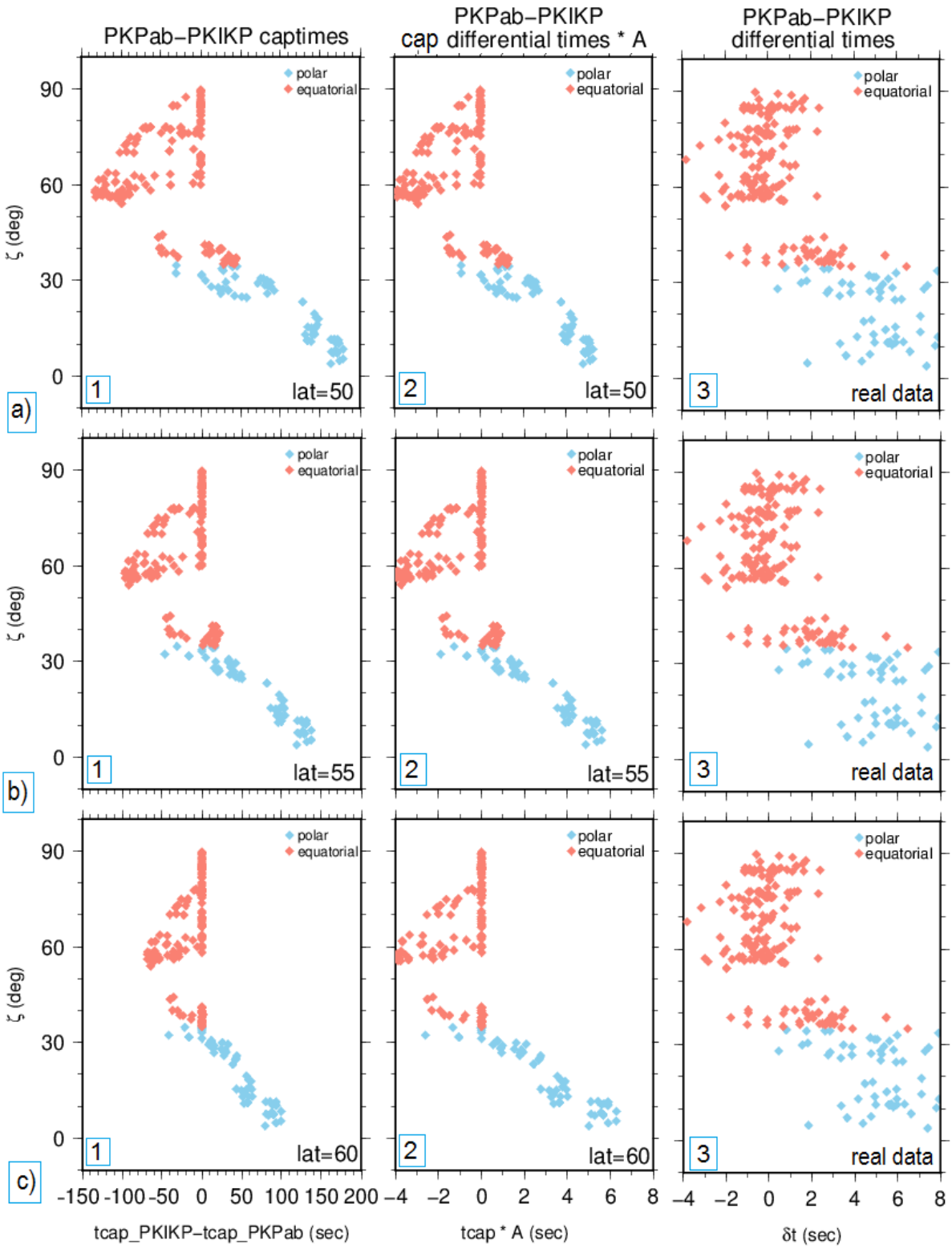

Figure 4.8: *Travel time difference between PKPab and PKIKP for time spent in a cap with latitudes of (a) 50°, (b) 55° and (c) 60° as a function of ζ between the ray path in the inner core and Earth's rotation axis. The differential times of the real data (3), the cap differential times multiplied by the average $\overline{A}_{cap}$ parameter (for $\overline{A}$ values see table 4.3) (2) and the cap differential times (1) are plotted as a function of ζ.*

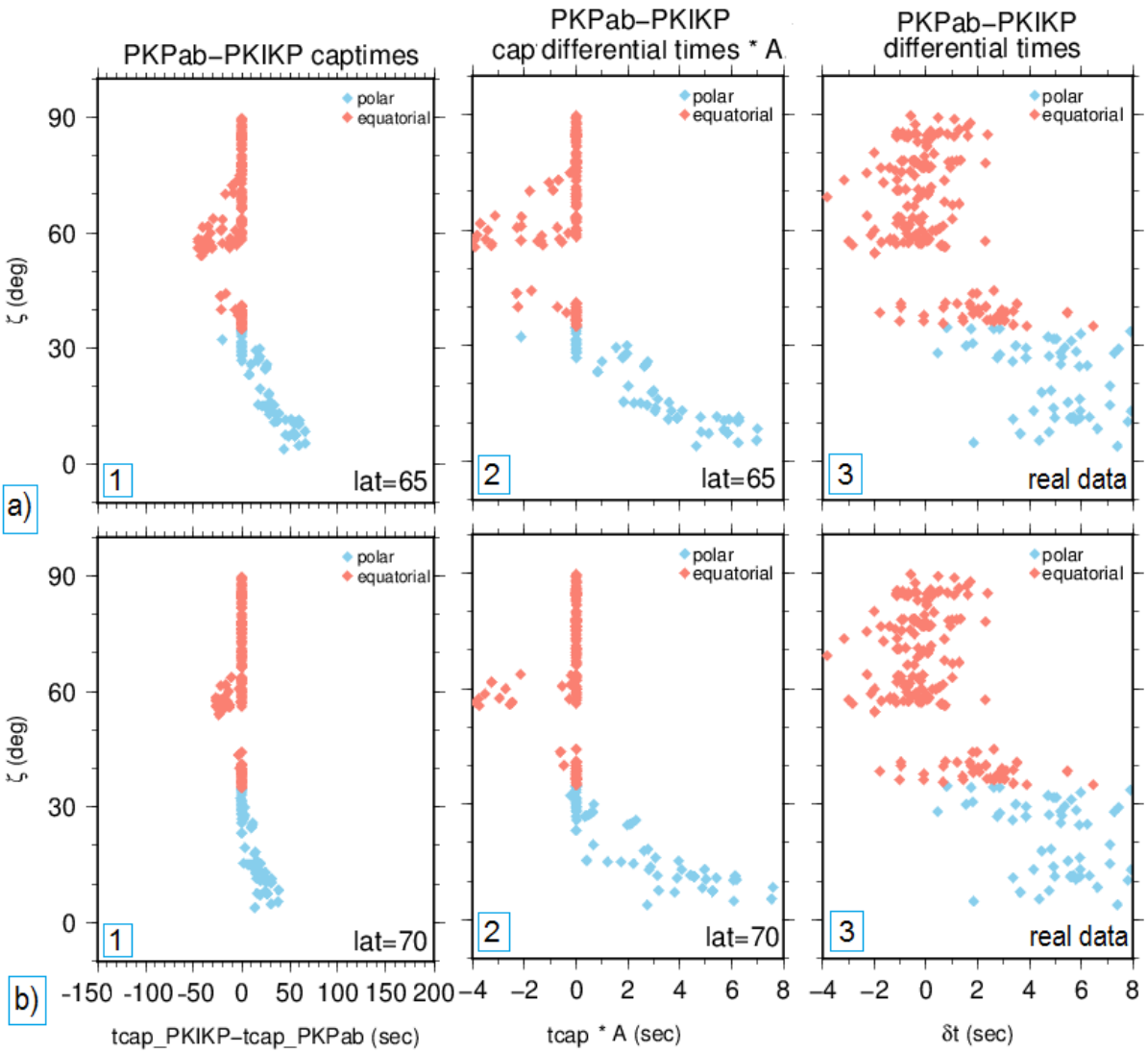

Figure 4.9: *Travel time difference between PKPab and PKIKP for time spend in a cap with latitudes of (a) 65° and (b) 70° as a function of ζ between the ray path in the inner core and Earth's rotation axis. The differential times of the real data (3), the cap differential times multiplied by the average $\overline{A}_{cap}$ parameter (for $\overline{A}$ values see table 4.3) (2) and the cap differential times (1) are plotted as a function of ζ.*

As before, we also investigate a separate north or south cap (figure 4.10). For both models, some equatorial waves have negative cap differential times and polar haves have positive cap differential times. For cap differential times multiplied by $\overline{A}_{cap}$ (δt_{cap}) the largest value is ±7 sec for the south cap model and only ±3 sec for the north model (figures 4.10a2 and b2). For the north cap model a large number of PKPab waves spend more time in caps than the PKPdf waves, leading to negative cap times (figure 4.10a) and a very high misfit compared to other models (table 4.3). Therefore, the north cap model is not pursued further.

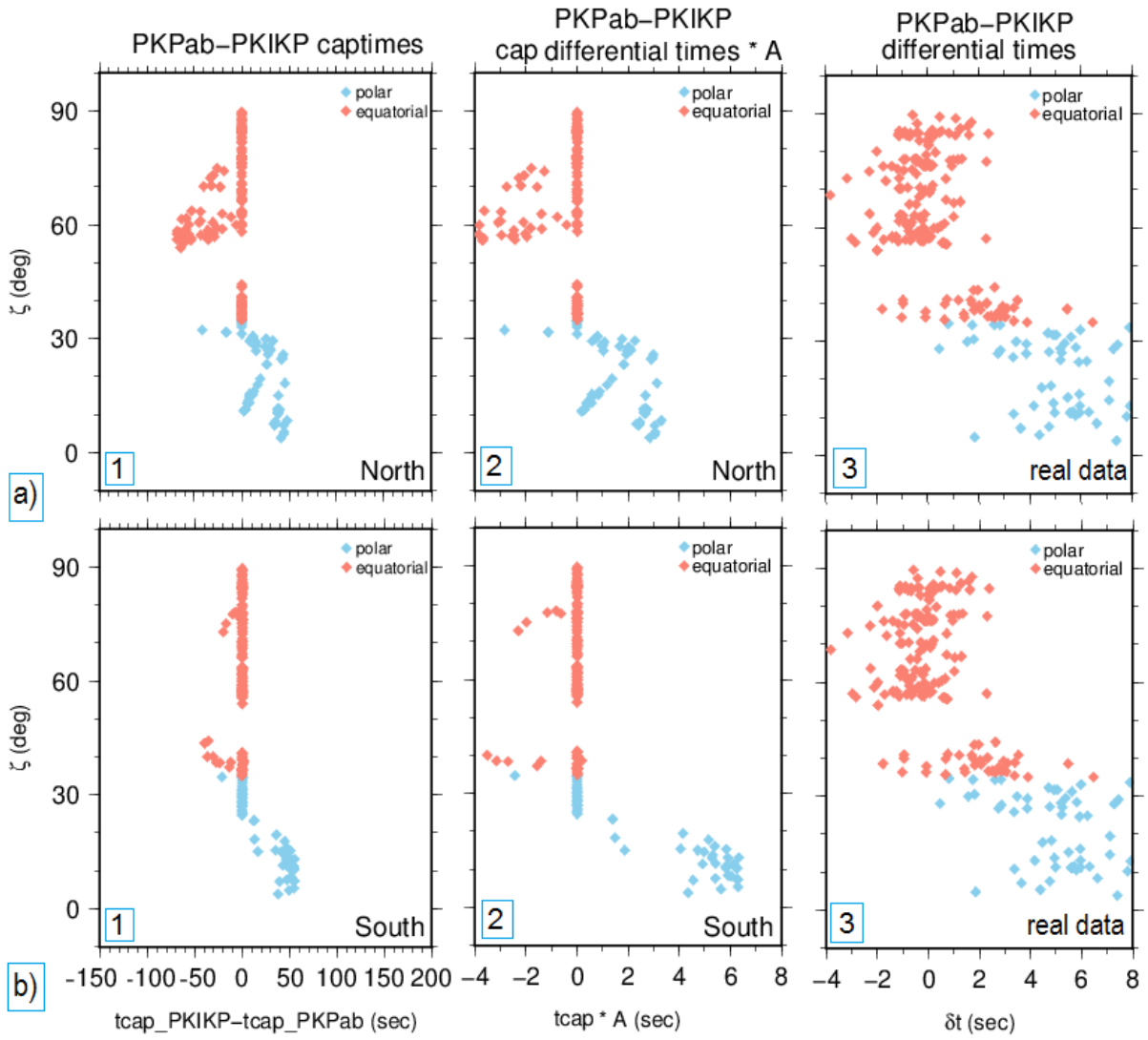

Figure 4.10: *Travel time difference between PKPab and PKIKP for time spent in a separate (a) north cap and (b) south cap as a function of ζ between the ray path in the inner core and Earth's rotation axis. The differential times of the real data (3), the cap differential times multiplied by the $\overline{A}_{cap}$ parameter (2) and the cap differential times (1) are plotted as a function of ζ. The caps have a cap boundary latitude of 60°.*

The PKPab-PKPdf dataset contains events with PKIKP waves that have an angle ζ<20° with the Earth's rotation axis and they reach from the most northern part of the Earth to Antarctica (table 4.1). These data points cause a broader range in ζ for polar waves. Therefore, the PKPab-PKPdf dataset has also been plotted without polar waves with ζ<20°, both for the real data as well as for polar caps with a boundary latitude of 60° north and south (figure 4.11). Without these polar waves, the scattering for polar waves for the cap model has disappeared and for the real data the scattering for the polar waves has decreased.

Table 4.1: Locations and dates of events with exceptionally low zeta (ζ<20°) values

Event	Year
Russia, east of Severnaya Zemlya	1992
Arctic ocean	2008
Baffin Bay	2009
Eastern Siberia Russia	2013

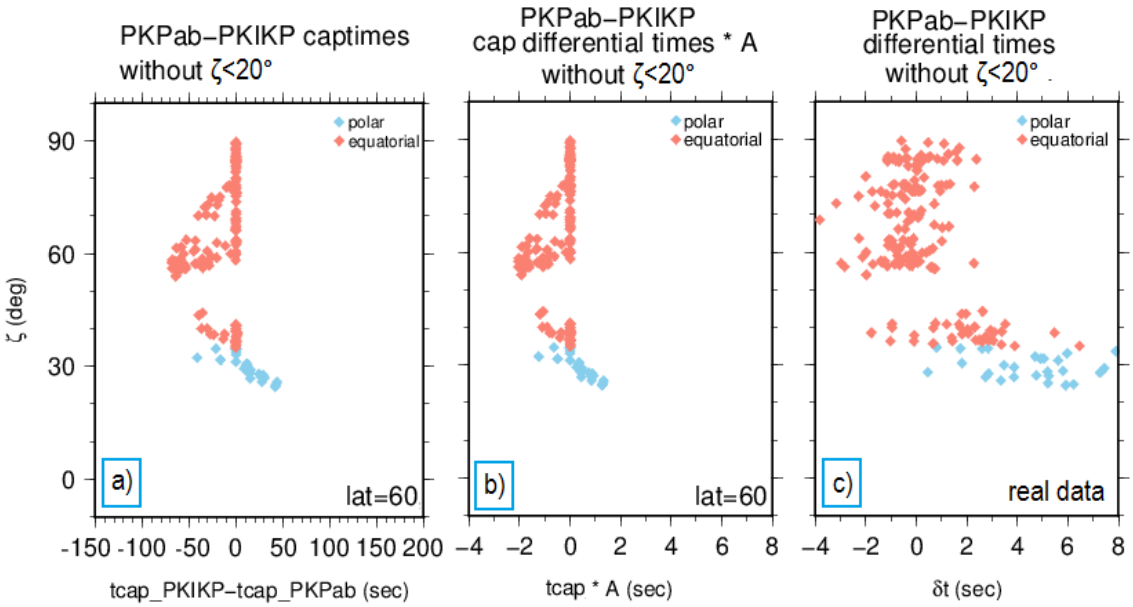

Figure 4.11: *a)Travel time difference between PKPab and PKIKP and b) the cap differential times multiplied by the $\overline{A}_{cap}$ parameter, for time spend in polar caps with a latitude of 60° as a function of $\zeta > 20°$. In figure c) the real PKPab-PKPdf differential time data is shown for ζ>20°.*

4.3 Tangent cylinder

We next investigate the alternative tangent cylinder model. The tangent cylinder is defined as a distinct region within the outer core, tangent to the inner core and intersecting the core surface at a latitude of ~69.5°. The cylinder has the same radius as the inner core (Hulot et al. (2002)). If the velocities of the P-waves are higher in the tangent cylinder than the surrounding outer core, polar PKPdf waves may arrive earlier than expected and therefore explains the data. If indeed the PKPab or PKPbc waves spend less time in these regions than the PKPdf wave, it explains why for these outer core waves anomalous arrival times are not observed. The cylinder differential times are calculated with the following equation (4.2)):

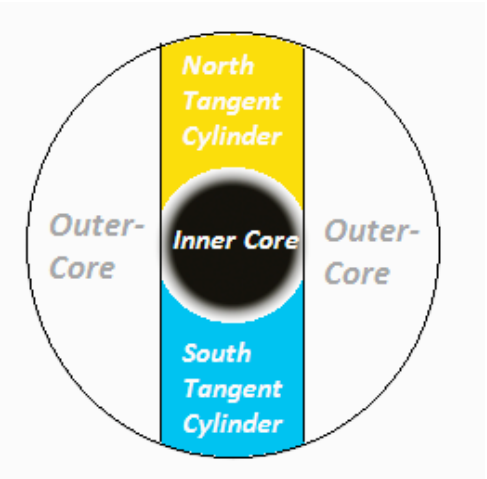

Figure 4.12: *The outer and inner core where the orange-yellowish part indicates the north part and the blue part the south part of the cylinder separated by the inner core.*

$$t_{cyl} = t_{(cyl\_PKPdf)} - t_{(cyl\_PKPbc/ab)} \tag{4.2}$$

We obtain positive cylinder differential times for polar waves, and negative differential times and differential times close to zero, for equatorial waves. This corresponds to the PKPab-PKPdf real data differential times and, apart from the large negative cylinder differential times, to the PKPbc-PKPdf real data differential times. For both the PKPbc-PKPdf and PKPab-PKPdf dataset the tangent cylinder model is separated into a north and south part of the cylinder to check if separate models fit better with the real data. The inner core separates both parts (figure 4.12). As done for the polar cap models, we fit the tangent cylinder model with the real PKPbc-PKPdf/ab data by the A_{cyl} parameter in equation 2.2. The average parameter $\overline{A}_{cyl}$ is then multiplied by all tangent cylinder differential times (equation 2.6) and plotted as a function of ζ, in order to get the differential times of the models and the real data in the same order of magnitude.

4.3.1 Tangent cylinder model for PKPbc dataset

PKPdf polar waves spend more time in the tangent cylinder than PKPbc polar waves. For equatorial waves, on the other hand, we find that either the PKPdf waves spend about the same amount of time in the tangent cylinder or the PKPbc spend more time in the tangent cylinder, resulting in negative tangent cylinder differential times (figure 4.13a and b). Here, we see that especially the negative cylinder times, for equatorial waves, are not seen in the real data. Still, the misfit of this model with the PKPbc-PKPdf differential times is low and therefore the tangent cylinder model fits the real data well.

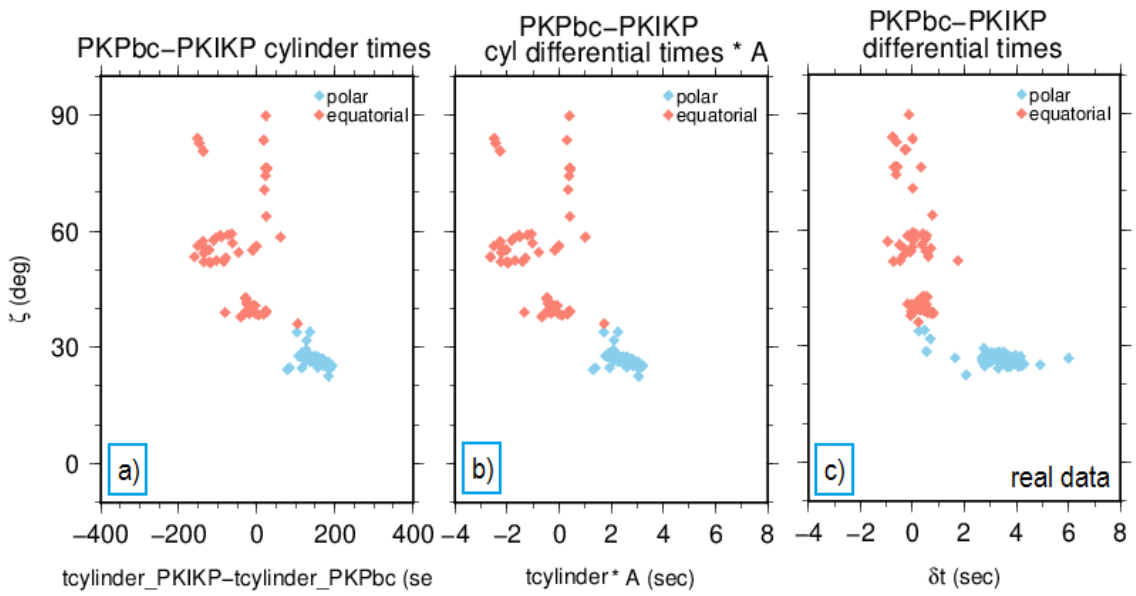

Figure 4.13: *The (a) tangent cylinder differential times between PKPdf (PKIKP) and PKPbc, (b) the cylinder differential times multiplied by the average $\overline{A}_{cyl}$ parameter (for $\overline{A}$ values see table 4.2) and (c) the real data differential times of PKPdf and PKPbc are plotted as a function of ζ.*

For the north part of the cylinder (figure 4.14a), we find that equatorial waves with a ζ=±55° show negative cylinder time difference, hence PKPbc waves spend more time in the upper part of the tangent cylinder than PKPdf waves. PKPdf polar waves, on the other hand, spend more time in the north part than PKPbc waves, leading to an increase in the tangent cylinder differential time when ζ decreases. For the south part of the tangent cylinder (figure 4.14b), negative cylinder differential times are observed when cylinder differential times are plotted with the same scale as the real PKPbc-PKPdf data (figure 4.14b2). Still, the north part of the tangent cylinder has the most similarities with the real data compared to the south cap model and therefore this model has a lower misfit (table 4.2).

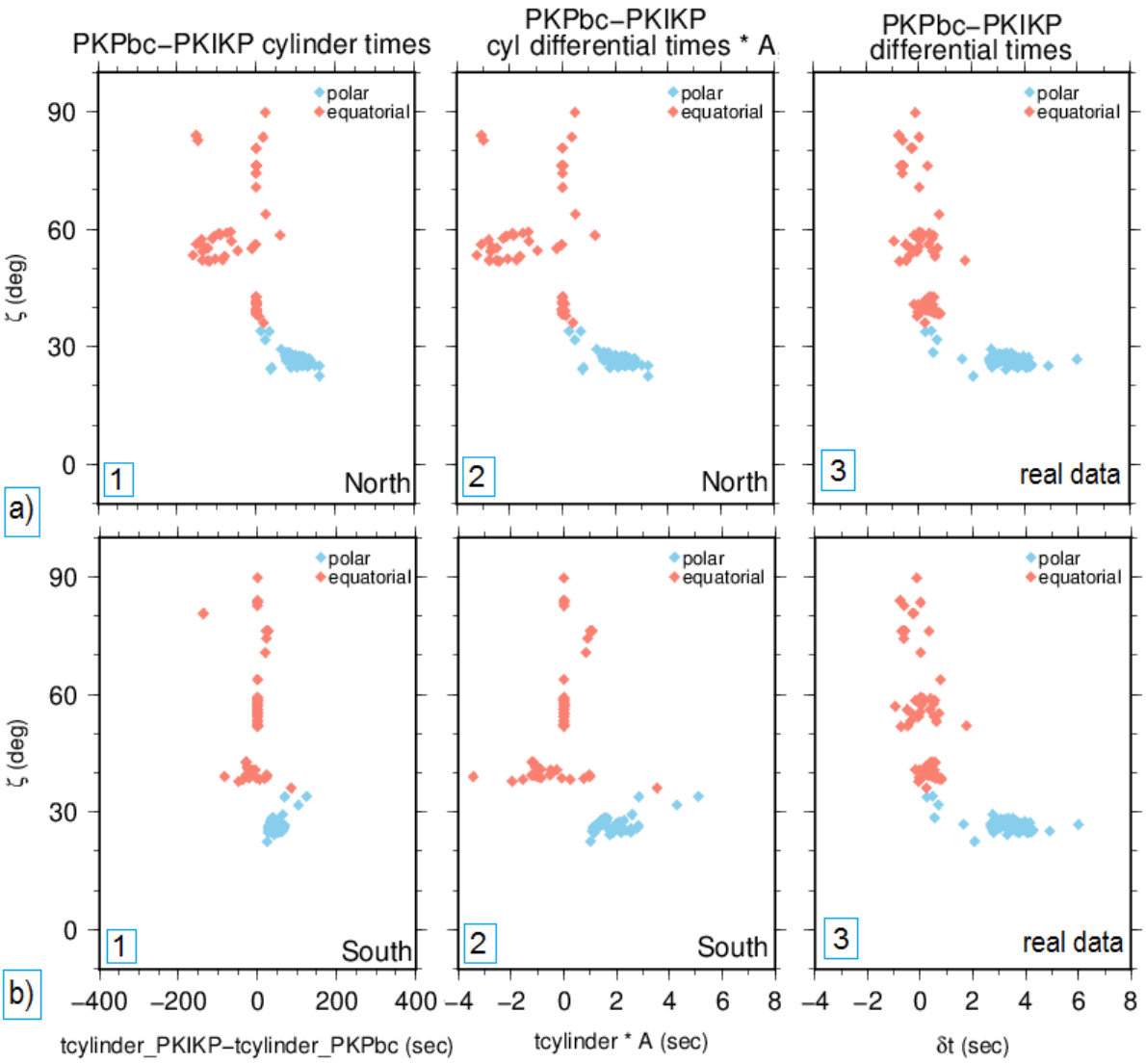

Figure 4.14: *(1) Tangent cylinder differential times, (2) fitted cylinder differential times and (3) differential travel times for PKPbc and PKPdf (PKIKP), are plotted as a function of zeta for a) the north part of the tangent cylinder and b) the south part of the tangent cylinder for the PKPbc-PKPdf dataset.*

4.3.2 Tangent cylinder model for PKPab dataset

When we plot PKPab-PKPdf cylinder differential times, multiplied by the average $\overline{A}_{cyl}$ parameter, as a function of ζ (figure 4.15b) we find a "curve" shape in the model times, just as is observed in the differential times of the real PKPab-PKPdf data (figure 4.15c). A smooth trend is observed of increasing cylinder differential times when ζ decreases. Some equatorial PKPab waves spend more time in the cylinder than the corresponding equatorial PKPdf waves, however since some differential times of the data are also negative, a few negative cylinder differential times explain the data (figure 4.15b and c). The cylinder differential times (figure 4.15b) and the real data (figure 4.15c) fit well, therefore the misfit of the tangent cylinder model for the PKPab-PKPdf dataset is low (table 4.3).

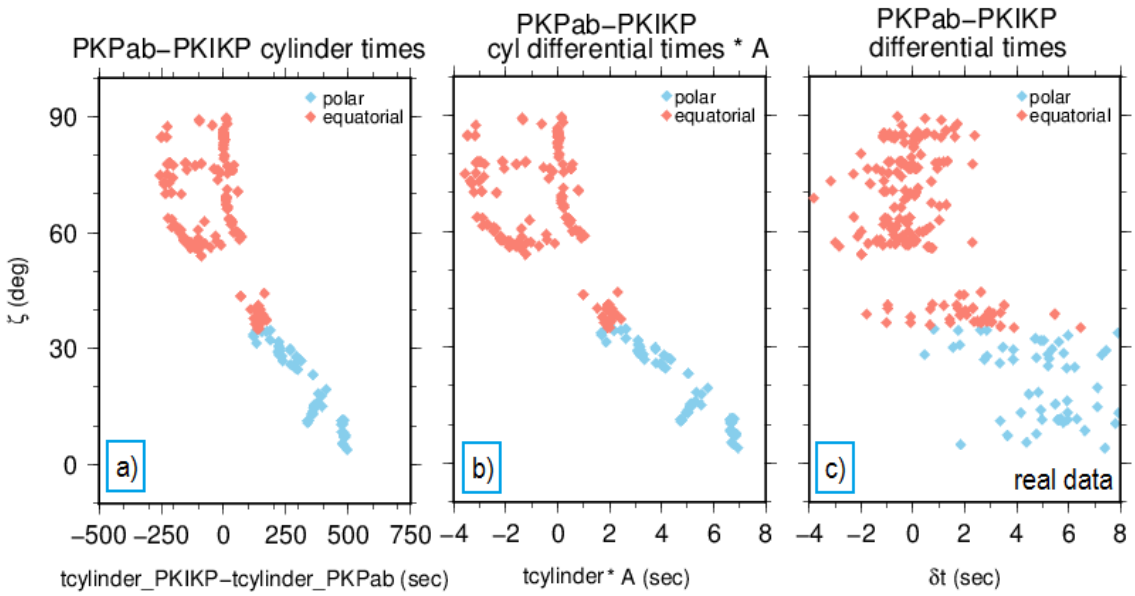

Figure 4.15: *(a) Tangent cylinder differential times, (b) fitted cylinder differential times and (c) differential travel times for PKPab and PKPdf (PKIKP), are plotted as a function of ζ. The "curved" structure is observed for this model and fits well with the real PKPab-PKPdf data.*

As before, the cylinder is separated in a north and south part. The "curve" feature is for both these models not clearly visible (figure 4.16a and b). For the south part of the cylinder, there is less scattering for the equatorial waves than for only the north part of the tangent cylinder (figure 4.16a2 and b2). The cylinder differential times of the south part cylinder, fit better with the real PKPab-PKPdf differential times and therefore the misfit is lower than for the north part only. The fit is best when the north and south part are not separated, as described above (table 4.3).

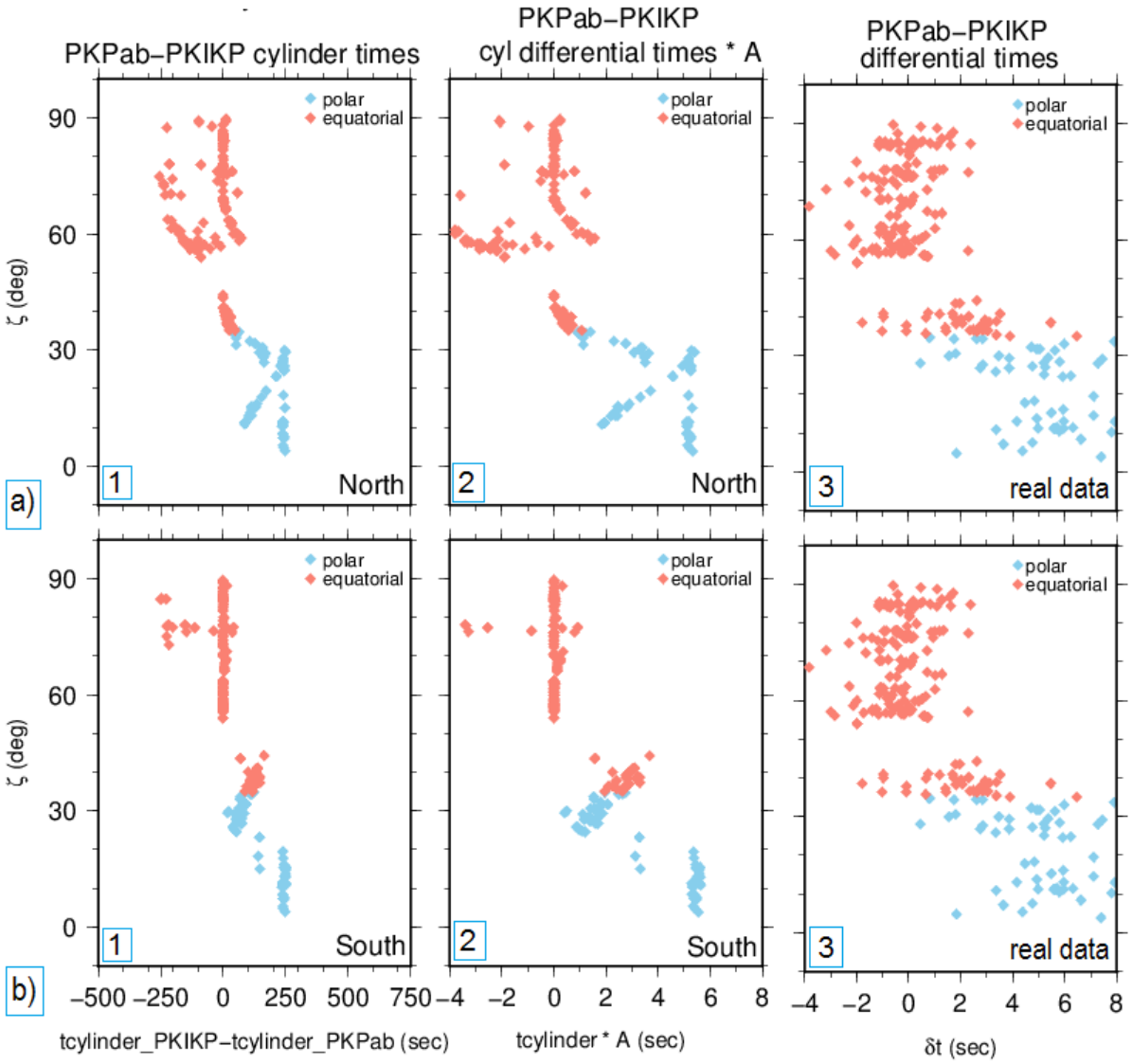

Figure 4.16: *(1) Tangent cylinder differential times, (2) fitted cylinder differential times and (3) differential travel times for PKPab and PKPdf (PKIKP), are plotted as a function of ζ for a) the north part of the tangent cylinder and b) the south part of the tangent cylinder for the PKPab-PKPdf dataset.*

4.4 Hemispheres

Previous studies found hemispherical structure in body wave observations for the inner core (Tanaka and Hamaguchi (1997)). We divide the Earth in an eastern hemisphere, from longitudes 0° to 180°, and a western hemisphere, from longitudes -180° to 0°. In order to investigate where the positive and negative cap and cylinder times appear, we plot the cap and cylinder time differences between PKPdf and PKPbc/ab waves and the real data differential times, as a function of turning longitude (figures 4.17 - 4.20). For the PKPbc-PKPdf dataset the polar waves have positive cap differential times in the western hemisphere and cap differential times around zero for the eastern hemisphere (figure 4.17a). This means that the PKPdf (PKIKP) waves spend more time in the caps than PKPbc waves if they pass through the western hemisphere and PKPdf polar waves that spend similar time in the caps as PKPbc waves or no time at all, pass the eastern hemisphere. This observation is in agreement with the real data differential times (figure 4.17b). This would be able to explain the hemispherical differences previously observed in the inner core. For the tangent cylinder model, the hemispherical differences are less clear, but for the eastern hemisphere the cylinder differential times are lower than in the western hemisphere indicating some hemispherical differences (figure 4.18a). For the PKPab-PKPdf dataset, the real data shows for the eastern hemisphere higher differential times for equatorial waves than in the western hemisphere (figure 4.20b). This observation is partly recognised for the tangent cylinder model, apart from some negative cylinder differential times, in figure 4.20a and is not observed for the polar caps model (figure 4.19a). Negative differential times of equatorial waves from the real PKPab-PKPdf data occur in the western hemisphere and can be explained by both the cap model and the cylinder model (figures 4.19a and 4.20a). These observations also argue for hemispherical differences, but where in the core these differences occur, remains questionable.

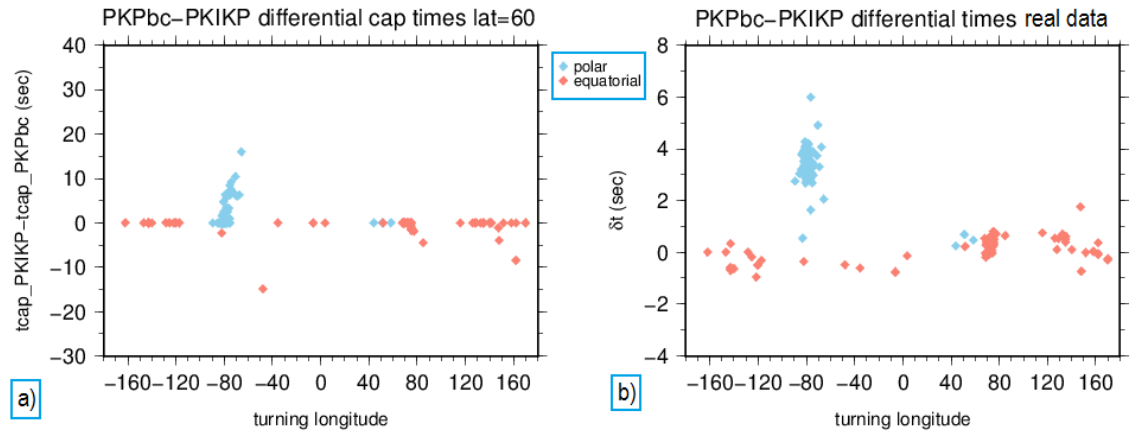

Figure 4.17: *For the PKPbc-PKPdf dataset we plot the (a) cap differential times and (b) the differential times of the real data as a function of turning longitude to see where in the core the negative and positive differential times occur. Figure (a) has a cap boundary latitude of 60°.*

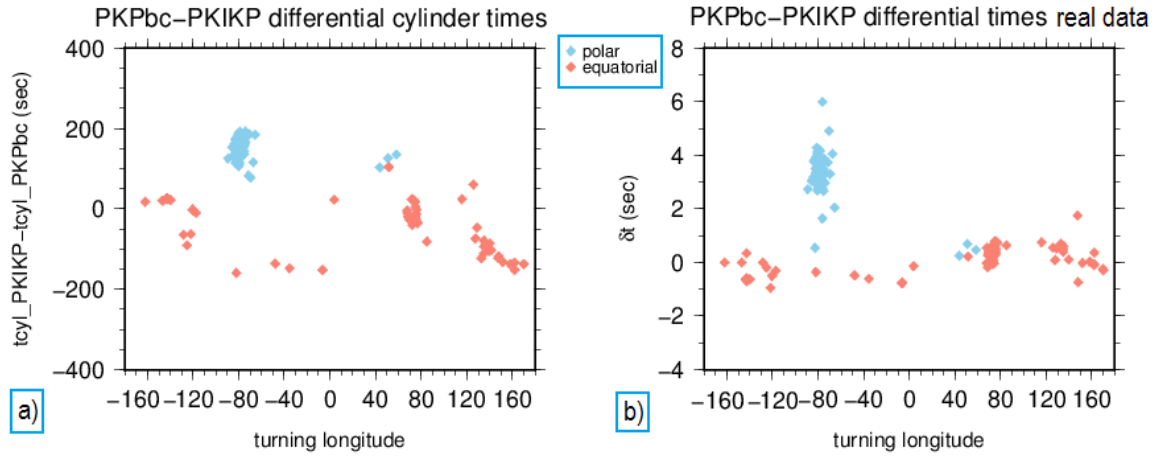

Figure 4.18: *We plotted the PKPbc-PKPdf dataset with the (a) cylinder differential times and the (b) real data differential times as a function of turning longitude.*

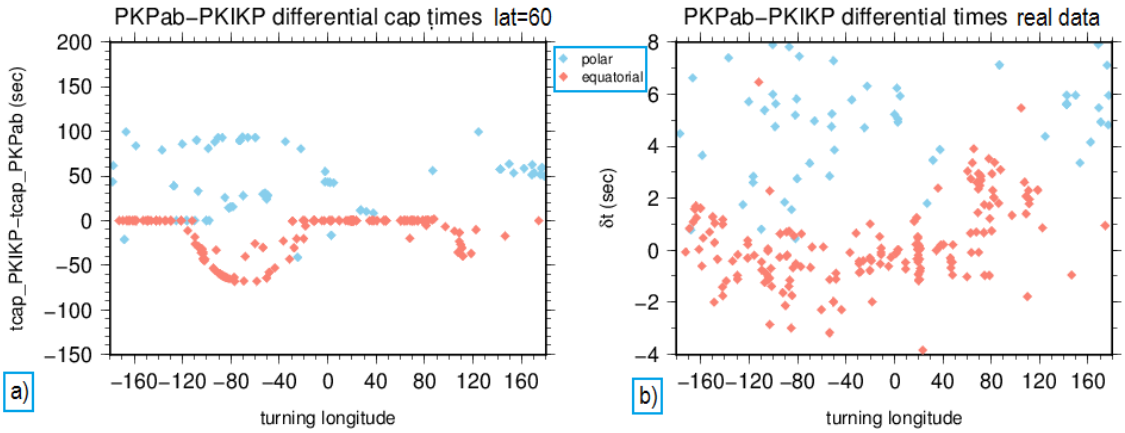

Figure 4.19: *For the PKPab-PKPdf dataset we plotted the (a) cap differential times and the (b) real data differential times as a function of turning longitude. The cap model has a boundary latitude of 60°*

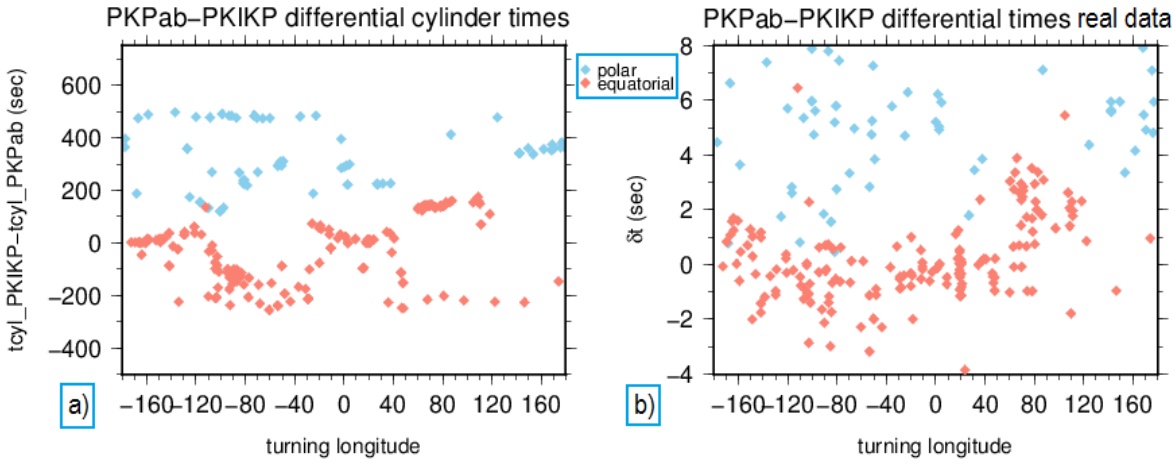

Figure 4.20: *We plotted the PKPab-PKPdf dataset with the (a) tangent cylinder differential times and the (b) real data differential times as a function of turning longitude.*

4.5 Inner core anisotropy

We also need to compare the tangent cylinder and polar caps models with the generally accepted 'inner core anisotropy' model. Inner core anisotropy is fitted by equation 2.4 via A, B and C with the PKPbc-PKPdf and PKPab-PKPdf datasets. The A, B and C values for the best fit are given in table 4.2 and 4.3. The red line in figure 4.21 and 4.22 shows the inner core anisotropy model fitting the data. The red line shows the same "curve" feature in the differential times over time spend in the inner core as PKPab-PKPdf data. The same accounts for the PKPbc-PKPdf dataset. Therefore, inner core anisotropy has a low misfit with the data.

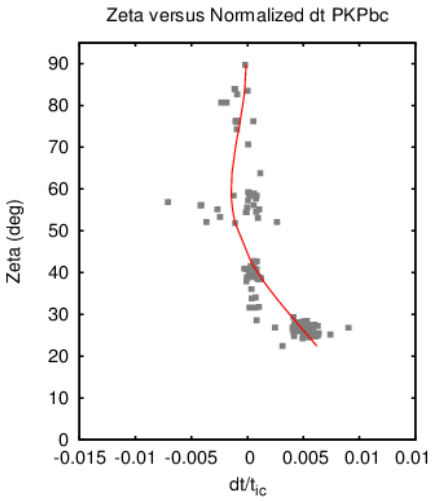

Figure 4.21: *The differential times over time in the inner core of the PKPbc-PKPdf dataset are plotted as a function of ζ. The red line indicates the fitted inner core anisotropy model.*

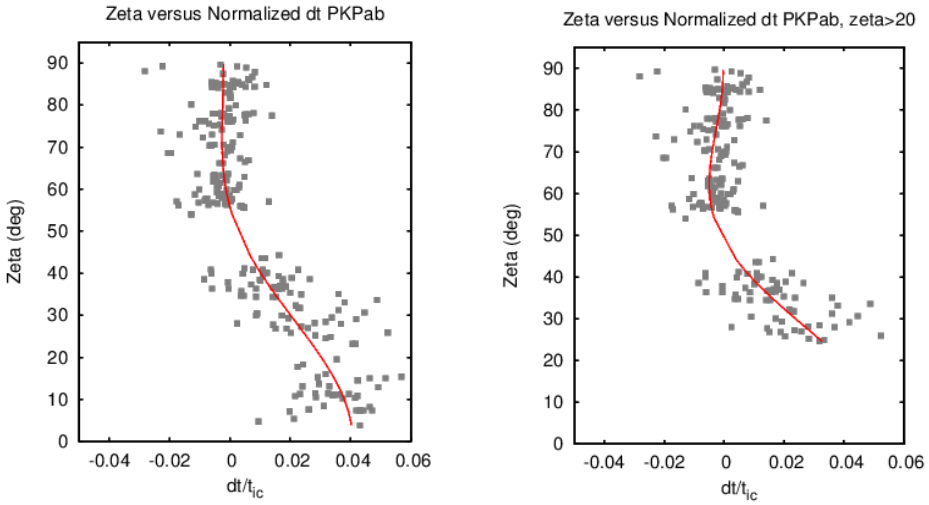

(a) (b)

Figure 4.22: *(a) The differential times over time in the inner core and (b) the differential time over time in the inner core for ζ values larger than 20° of the PKPab-PKPdf dataset, are plotted as a function of ζ. The red lines indicate the fitted inner core anisotropy model.*

4.6 Model fit

To determine which models fit best with the data, the misfit (equation 2.8) is compared to a misfit value where no waves pass through a cap or cylinder, causing a very high misfit value (2.545 for the PKPab-PKPdf dataset and 1.9406 for the PKPbc-PKPdf dataset) since it does not fit with the data. To determine the variance of the model misfits with the reference misfit, the following equation is used (4.3):

$$variance = \frac{misfit_{ref} - misfit_{model}}{misfit_{ref}} \tag{4.3}$$

This way the variance will be between 0 and 1. If the variance is close to one, the model has a better fit with the real data and if the variance is close to zero, the model does not fit the data well. For all models mentioned above, the average model parameter $\overline{A}_{cyl/cap}$, the misfit and variance are determined for the PKPab-PKPdf and PKPbc-PKPdf datasets and shown in tables 4.2 and 4.3. For the PKPbc-PKPdf and the PKPab-PKPdf datasets, the model that has the highest variance is inner core anisotropy. For the PKPbc-PKPdf dataset this is followed by the polar cap model with a latitude of 50° (-50°) and the tangent cylinder model (table 4.2). From all cap sizes, the cap with the largest thickness (812.06 km) is favored.

Table 4.2: *Model parameters and Misfit for PKPbc-PKPdf*

Model	A	misfit	variance [0-1]	Best fit
Reference		1.9406	0	11
Cap lat 50	0.12321	1.157	0.404	2
Cap lat 55	0.19178	1.376	0.291	5
Cap lat 60	0.36999	1.689	0.130	8
Cap lat 65	0.79224	1.891	0.026	9
Cap North	0.38555	1.635	0.157	7
Cap South	-0.24848	1.918	0.012	10
Tangent cylinder	0.01640	1.207	0.378	3
Tangent cylinder North part	0.020355	1.283	0.339	4
Tangent cylinder South part	0.04124	1.495	0.230	6
Inner core anisotropy	A=-0.000128 B=-0.0105593 C=0.0210117	0.530	0.727	1

For the PKPab-PKPdf dataset, the tangent cylinder model also shows a well fit with the data, since the variance values are relatively large. In table 4.3 the misfit is also calculated for ζ values >20° for the PKPab-PKPdf dataset. Since the scattering decreases for the polar waves differential times, the variance values of the cap model with boundary latitude of 60° and the tangent cylinder model improve (table 4.3). For inner core anisotropy, no changes are observed when ζ<20 are eliminated. Even though the

misfits decrease when these events are eliminated, they are good data and can therefore not be ignored. The events causing these paths with exceptionally low zeta values are shown in table 4.1.

Since the PKPab waves travel a more different path than the PKPdf waves compared to PKPbc waves, it is more likely that PKPab waves pass the tangent cylinder or polar caps, even if the PKPdf (PKIKP) waves do not pass these regions, compared to PKPbc waves. If PKPbc waves pass the cylinder or polar caps, it is likely that PKPdf waves also pass this distinct region and hence the cap or cylinder time difference between these waves will be small. The time differences for as well the caps as the tangent cylinder are indeed smaller values for the PKPbc-PKPdf dataset than the PKPab-PKPdf dataset (figure 4.6 and 4.8).

Table 4.3: *Model parameters and Misfit for PKPab-PKPdf*

Model	A	misfit	variance [0-1]	Best fit
Reference		2.545	0	12
Cap lat 50	0.02947	2.011	0.210	8
Cap lat 55	0.04083	1.992	0.217	6
Cap lat 60	0.06329	2.035	0.200	7
Cap lat 65	0.09931	2.058	0.191	9
Cap lat 70	0.19147	2.126	0.165	10
Cap North	0.06884	2.399	0.057	11
Cap South	0.11501	1.978	0.222	5
Tangent cylinder	0.01401	1.572	0.382	2
Tangent cylinder North part	0.02149	1.971	0.226	4
Tangent cylinder South part	0.02238	1.737	0.317	3
Inner core anisotropy	A=-0.00215 B=-0.00982 C=0.0527	1.185	0.534	1
Cap lat 60 with ζ>20°	0.030055	1.735	0.318	*3*
Tangent cylinder with ζ>20°	0.01165	1.500	0.411	*2*
Inner core anisotropy without polar (ζ<20°)	A=-0.000291 B=-0.0436 C=0.100931	1.186	0.534	*1*

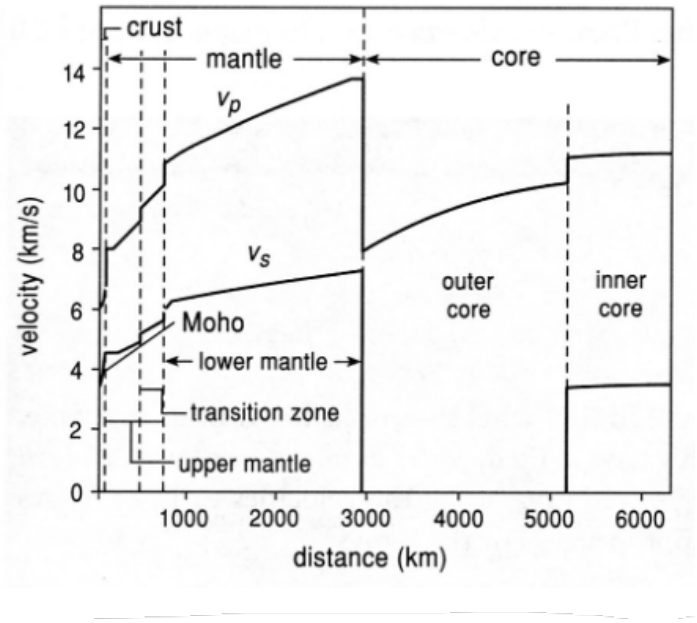

Figure 4.23: *Velocity of P-wave versus depth in the Earth's layers.*

To determine the P-wave velocities within the tangent cylinder and the polar caps, the average model parameter $\overline{A}_{cap/cyl}$ from tables 4.3 and 4.2 is used (equation 4.4). The differential times, over the time spend in the cap or cylinder is equivalent to the velocity perturbation in the cap or cylinder, over the P-wave velocity in the outer core:

$$\frac{\delta V}{V_p} = \frac{\delta t_{cap/cyl}}{t_{cap/cyl}} = \overline{A}_{cap/cyl} \tag{4.4}$$

With Vp as the P-wave velocity and δV as the velocity perturbation in the cap or cylinder. From figure 4.23 the absolute velocity of the P-waves through the outer core is used. For polar caps, hence near the core-mantle boundary, the P-wave velocity is approximately 8 km/s and for the tangent cylinder an average is taken of approximately 10km/s. With equation 4.4 and the outer core velocities we calculated the velocity increase or decrease and absolute P-wave velocities within the cap or tangent cylinder and are shown in table 4.4.

Table 4.4: *The velocity increase, absolute velocity increase and absolute velocity for various outer core models*

Model + dataset	Velocity increase	Abs velocity increase	Abs velocity
Cap lat 50 PKPab	2.94%	0.24 km/s	8.24 km/s
Cap lat 50 PKPbc	12.32%	0.99 km/s	8.99 km/s
Cap lat 55 PKPab	4.08%	0.33 km/s	8.33 km/s
Cap lat 55 PKPbc	19.18%	1.53 km/s	9.53 km/s
Cap lat 60 PKPab	5.93%	0.47 km/s	8.47 km/s
Cap lat 60 PKPbc	37.00%	2.69 km/s	10.69 km/s
Cap lat 65 PKPab	9.93%	0.79 km/s	8.79 km/s
Cap lat 65 PKPbc	79.22%	6.34 km/s	14.34 km/s
Cap lat 70 PKPab	19.15%	1.53 km/s	9.53 km/s
Cap north PKPab	6.88%	0.55 km/s	8.55 km/s
Cap north PKPbc	38.56%	3.08 km/s	11.08 km/s
Cap south PKPab	11.50%	0.92 km/s	8.92 km/s
Cap south PKPbc	-24.85%	-1.99 km/s	6.012 km/s
Tangent cylinder PKPab	1.40%	0.13 km/s	9.13 km/s
Tangent cylinder PKPbc	1.64%	0.15 km/s	9.15 km/s
Tangent cylinder north PKPab	2.15%	0.19 km/s	9.19 km/s
Tangent cylinder north PKPbc	38.55%	3.47 km/s	12.47 km/s
Tangent cylinder south PKPab	2.24%	0.20 km/s	9.20 km/s
Tangent cylinder south PKPbc	4.12%	0.37 km/s	9.37 km/s
Cap lat 60 with z>20 PKPab	3.01%	0.24 km/s	8.24 km/s
Tangent cylinder with z>20 PKPab	1.17%	0.10 km/s	9.10 km/s
Inner core anisotropy PKPab	6.25%	PKPdf goes 0.56 km/s faster	9.56 km/s
Inner core anisotropy PKPab z>20	5.74%	PKPdf goes 0.51 km/s faster	9.51 km/s
Inner core anisotropy PKPbc	3.16%	PKPdf goes 0.28 km/s faster	9.28 km/s

The velocities determined for the polar cap and tangent cylinder models indicate an increase in P-wave velocities when passing the distinct region (table 4.4). It is geodynamically unlikely that the velocity increases by 79% for the PKPbc-PKPdf dataset, therefore the polar caps with a latitude of 65° (-65°) is not plausible. The same is true for the cap models with a latitude of 60°, 55°, 50°, only a north cap and only a south cap. The high velocity increases are mostly for the PKPbc-PKPdf dataset. Some cap size-models are realistic for the PKPab-PKPdf waves, since the increase is ±3-6%: caps with a latitude of 50°, 55° and 60°. Overall, the tangent cylinder model explains the data better, since the velocity increase is more sensible (<4% velocity increase). The model with the lowest misfit is the inner core anisotropy model. For our PKPab-PKPdf dataset there is 6.25% anisotropy, for the PKPab-PKPdf dataset with ζ>20° there is 5.74% anisotropy and for the PKPbc-PKPdf dataset there is only 3.16% anisotropy. This

is in agreement with Irving and Deuss (2011). This percentage indicates the velocity difference between polar and equatorial waves.

Chapter 5

Discussion

In this study, an "L-shape" feature for the PKPbc-PKPdf dataset and a "curve" feature for the PKPab-PKPdf dataset are also obtained for a model with a tangent cylinder or polar caps present in the outer core and no inner core anisotropy. We find that polar PKPdf waves spend more time in the cylinder and polar caps than polar PKPbc waves, therefore this explains why the polar PKPdf waves arrive sooner than predicted by the AK135 model (Kennett et al. (1995)).

One of the limitations of this project is that when manually picking the arrival times of the PKPdf, PKPbc and PKPab waves, uncertainties are generated of only a few seconds. Furthermore, since a few events have been used for this research, uneven sampling occurs and only several regions have been tested in the Earth. More data can be acquired for further research.

5.1 Models of this study

5.1.1 Polar cap model

We observe equatorial waves with negative cap time differences between PKPdf and PKPbc. For some situations (figure 5.1) PKPbc waves spend more time in the caps than the PKPdf waves and therefore deviate from the "L-shape" structure, visual in the real data. These datapoints are good data and cannot be ignored, making the polar cap theory less likely. Negative cap time differences are also observed for the PKPab-PKPdf dataset, however some negative cap time explain the negative differential times of the real PKPab-PKPdf data (figure 5.2). For the PKPbc-PKPdf dataset the cap model with a boundary latitude of 65°, shows a velocity increase of 79%. Other velocity increases are also unrealistically high for the polar cap models (table 4.4). The high misfits, variances close to zero and unrealistic velocity increases, show that the polar cap model does not explain the data well and therefore should not be pursued further.

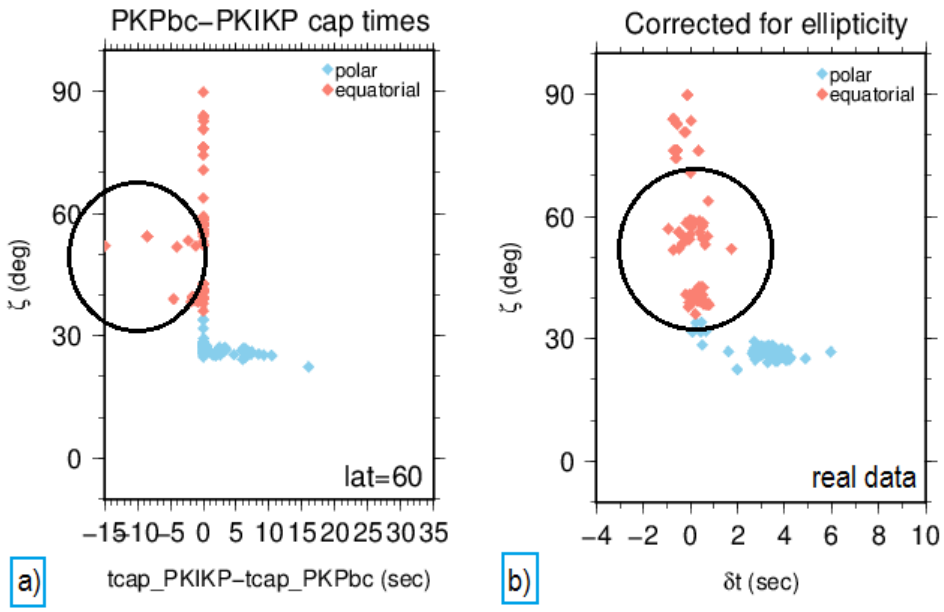

Figure 5.1: *a) shows for a cap of latitude 60° the cap time difference between PKPdf and PKPbc waves. An "L-shape" feature is observed, however, a few deviating points show negative cap time differences (indicated by the black circle). The PKPbc waves spend more time in the caps than the PKPdf (PKIKP) waves. This is not observed in the real data (b). The differential times of the PKPbc-PKPdf dataset as a function of zeta are shown in b).*

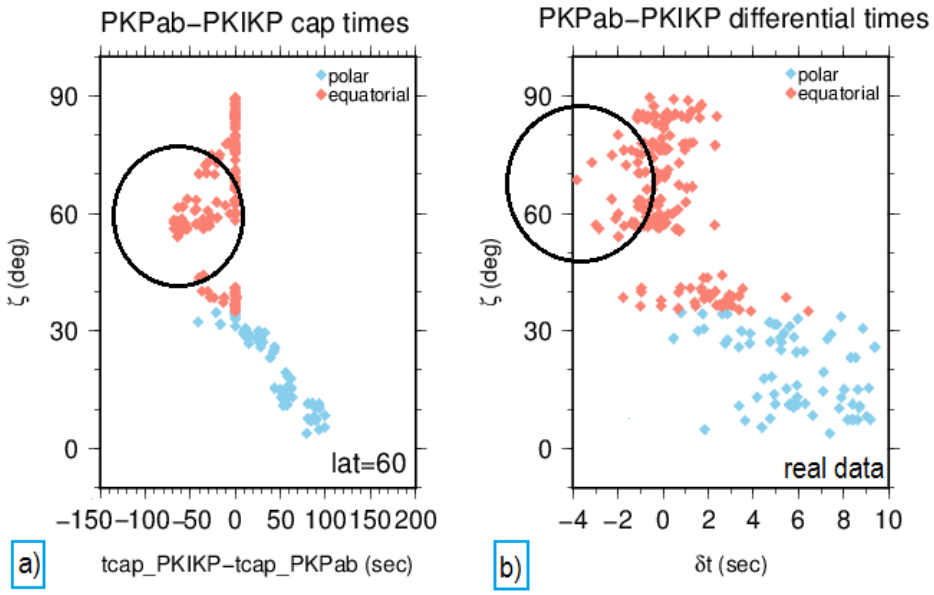

Figure 5.2: *a) shows for a cap of latitude 60° the cap time difference between PKPdf and PKPab waves. A "curve" feature is in both a) and b) observed, however, deviating points show negative cap time differences (indicated by the black circle). The PKPab waves spend more time in the caps than the PKPdf (PKIKP) waves. Some of these negative cap time difference do explain the data, but more cap time difference are negative than differential times of the real PKPab-PKPdf dataset (a). The differential times of the PKPab-PKPdf dataset as a function of ζ are shown in b).*

5.1.2 Tangent cylinder model

In plots where the cylinder time differences are plotted as a function of ζ, there are a lot of events where the PKPbc spends more time in the cylinder than the PKPdf wave (figure 4.13). In fact, for the PKPbc-PKPdf dataset, more equatorial waves show negative cylinder time differences than zero values (which was expected). These negative cylinder time differences deviate from the expected "L-shape" feature as seen in the real PKPbc-PKPdf differential times, which is in contrast to the tangent cylinder model. The scattering, for equatorial waves, in cylinder time differences is also visible for the PKPab-PKPdf dataset. However, more negative cylinder time differences explain the negative differential times in the real PKPab-PKPdf data than was observed for the polar cap models (figure 4.15). From table 4.2 and 4.3 the misfits of the tangent cylinder models are low compared to the polar cap models. The velocity increase within the tangent cylinder in the outer core are for the PKPab-PKPdf dataset plausible, they are found to be ±1-2% increase. These observations are favorable for the tangent cylinder model.

Even though the misfit is low and the velocity increase within the tangent cylinder is realistic, the extreme negative cylinder time difference (especially for the PKPbc dataset) cannot be fully explained. We find that the large negative cylinder time differences are not caused by one event, in fact, every event with equatorial waves contain some stations with PKPbc/ab waves spending more time in the cylinder than PKPdf equatorial waves.

5.2 Hemispherical variations

Another question is the existence of hemispheres. Tanaka and Hamaguchi (1997) discovered that the inner core is divided in an anisotropic western hemisphere and an isotropic eastern hemisphere. Our datasets also show some evidence for the existence of the hemispheres; in figure 5.3b no polar wave PKPbc-PKPdf differential times are found with values higher than zero in the eastern hemisphere, only in the western hemisphere.

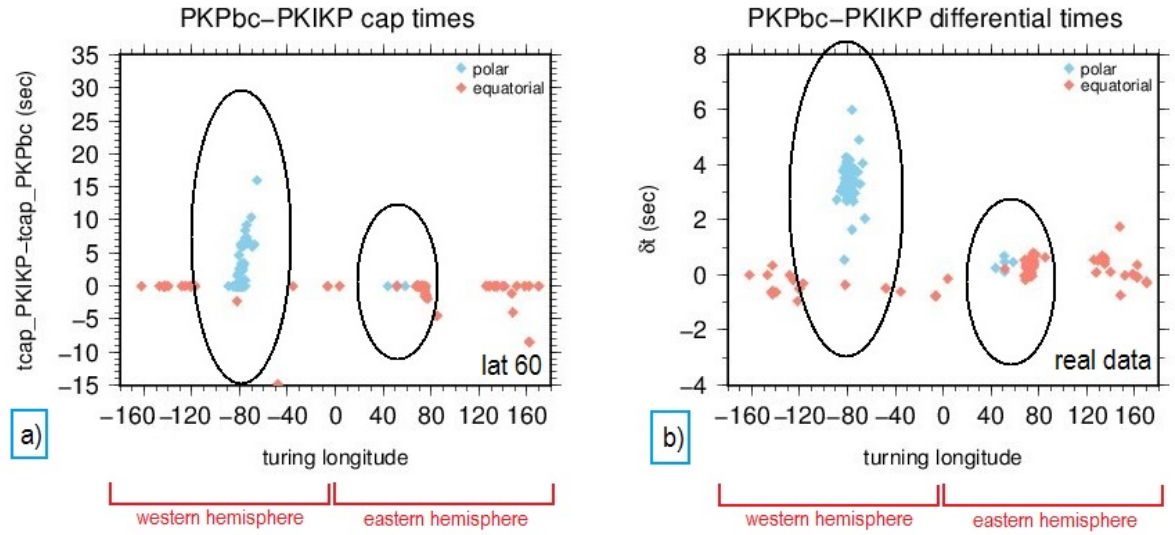

Figure 5.3: *a) the cap time difference, with a boundary latitude of 60°, between PKPdf and PKPbc are plotted as a function of turning longitude of the ray paths and b) shows the real data differential times of the PKPbc-PKPdf dataset as a function of turning longitude. It is observed that for both figures for the western hemisphere positive time differences are shown and for the eastern hemispheres the time differences for as well the cap times as the differential times are around zero.*

The "L-shape" feature in the data plots (figure 4.3) is therefore solely caused by polar waves that pass the western hemisphere. Previous studies interpreted this as only the western hemisphere, inside the inner core, being anisotropic. Interestingly, when we plot the cap time differences between the PKPdf and PKPbc waves against the turning longitude, we find that the waves passing the western hemispheres have highest cap time differences and the eastern hemisphere shows cap times close to zero for polar paths (5.3a). This is also observed for the PKPbc-PKPdf polar waves in the tangent cylinder model, where the cylinder differential times are higher values when passing the western hemisphere than the eastern hemisphere (figure 4.18). So, without hemispheres being present in our cap and cylinder model, the paths are such that it seems there are hemispheres. Thus, we should be careful interpreting the data as being hemispherical.

For equatorial waves, passing the eastern hemisphere, the PKPbc waves spend more time in the caps than PKPdf waves, causing negative cap time differences. This only occurs with equatorial waves passing through the eastern hemisphere, not the western. This observation contradicts the data.

For the equatorial PKPab-PKPbc waves, the differential times are a bit higher in the eastern hemisphere than in the western hemisphere, which is indicated by the black line in figure 5.4b. The same pattern is observed for cylinder time difference between PKPab and PKPdf waves (figure 5.4a), therefore the tangent cylinder model explains the PKPab-PKPdf dataset well and indicates hemispherical differences.

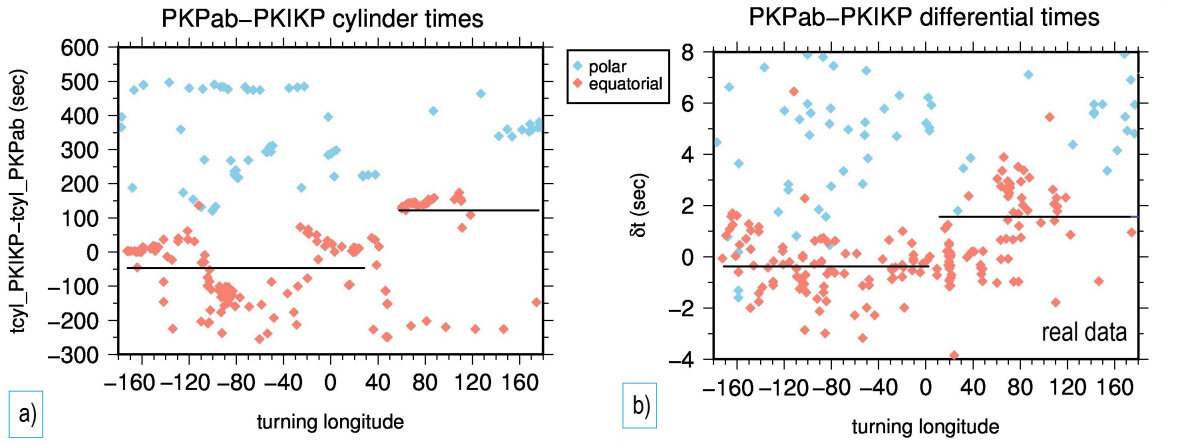

Figure 5.4: *a) the tangent cylinder time difference between PKPdf (PKIKP) and PKPab are plotted as a function of turning longitude of the ray paths and b) shows the real data differential times of the PKPab-PKPdf dataset as a function of turning longitude. For the eastern hemisphere in a) and b) higher differential time values for equatorial waves are observed compared to the differential times of the equatorial waves in the western hemisphere.*

Furthermore, all deviating equatorial differential times in the PKPab-PKPdf dataset, that should have a value near zero, have paths in the eastern hemisphere. Their differential times are high and deviate from the "curve" feature (5.4). However, they have a ζ value around 40°. Therefore, they are closer to the earth's rotation axis direction than to the equatorial direction and might be polar waves instead.

5.3 Comparison and considerations of models

Inner core anisotropy is generally accepted to explain the PKPbc-PKPdf/ab observations. Besides body-wave traveltime observations, anomalous splitting of core-sensitive free oscillations are best explained by inner core anisotropy. However, Bréger et al. (1999) suggested that heterogeneity in the D"-layer was responsible for the PKPab-PKPdf velocity differences as a function of ζ. Hrvoje et al. (2002) evaluated how much of the core-sensitive PKP travel-time data can be explained by mantle structure alone, and indeed a large amount of the PKPab-PKPdf data was explained by the mantle structure only. Ishii et al. (2002) suggested that the data can be explained by a combination of a simple inner core anisotropy model and mantle heterogeneities. One of the main issues with inner core anisotropy is that the modes that are most strongly split, are the normal modes sampling the top part of the inner core, which is assumed to be isotropic (Song and Helmberger (1998)). Here we discuss an alternative explanation, which was proposed by Romanowicz and Bréger (2000): "outer core structures can explain travel time differences between PKPbc-PKPdf and anomalous splitting of normal modes". For over 20 modes sensitive to core structure (except ${}_3S_2$), outer core structure improves the fits with respect to a mantle-only model. The outer core structure model, however, underpredicts the splitting of the ${}_3S_2$ mode. Romanowicz and Bréger (2000) found that the fit of the outer core models is at least as good as the fits of models with inner core anisotropy. Only when ${}_3S_2$ is included they obtain a better fit with inner core anisotropy models. The interpretation of core sensitive modes in terms of inner core anisotropy, therefore relies on one single mode. They state that light elements in the outer core are restricted to a distinct region like

the "tangent cylinder". Souriau et al. (2003) used PKPbc time residuals to find if anisotropy inside the tangent cylinder could explain the faster propagation time of these paths. They tested the north and south part separately, and found no differences. This is in accordance with this study, where we also found no major difference between the north and south part of the tangent cylinder when ζ is plotted against cylinder time differences.

Romanowicz and Bréger (2000) also found that the density structure is largest at the top of the core, this would be compatible with a stagnant layer at the top of the outer core to a maximum depth of 500 km (i.e. potential polar caps). However, in my study it is clear that the misfit of most cap sizes with both PKPbc-PKPdf and PKPab-PKPdf datasets is relatively large and the P-wave velocity increases in these stagnant polar regions, are unrealistically high, even for the thickness of 500 km (lat=~60°). It is therefore unlikely that polar caps in the liquid outer core explain the observed fast waves in the direction parallel to the rotation axis. Romanowicz and Bréger (2000) also show that models are preferred for heterogeneity that extends over a large thickness in the outer core instead. Therefore, they favor a tangent cylinder in the outer core, with a velocity increase inside the tangent cylinder of ±1%. They also found for PKPbc-PKPdf differential times an "L-shape" feature and for the PKPab-PKPdf differential times a "curve" feature present, when plotted as a function of ζ for the tangent cylinder model (figure 5.5). We found, like Romanowicz and Bréger (2000), that the tangent cylinder explains the PKPab-PKPdf and PKPbc-PKPdf datasets well; the misfit with both datasets is relatively low (in top 3 best fit) and the velocity increases from 1.40% for the PKPab dataset to 1.64% for the PKPbc dataset. These velocity increase are compatible with Romanowicz and Bréger (2000). However, inner core anisotropy is an even better fit.

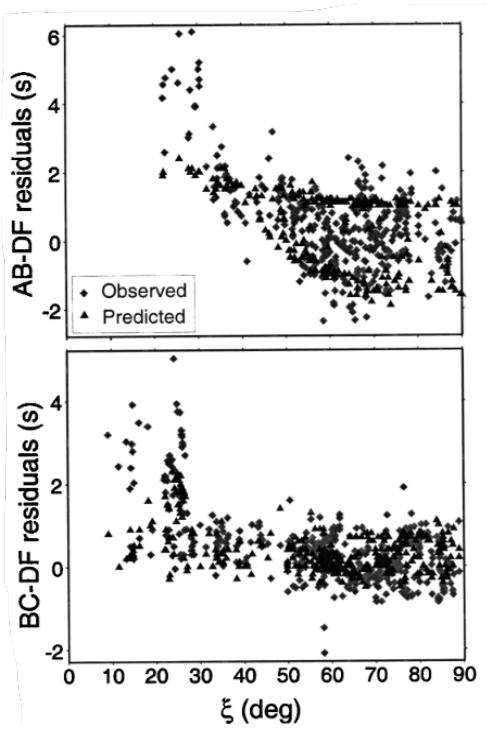

Figure 5.5: *observed and predicted differential times for PKP waves, for the tangent cylinder model by:*

Romanowicz and Bréger (2000)

The polar cap model requires heterogeneities at the top of the liquid core, beneath the core mantle boundary. These structures might be created by the ellipticity of the core-mantle boundary and resulted in light elements concentrating at the top of the liquid core due to inner core crystallization. The concentration of light elements will be unequally divided due to the rotation of the earth, which has also been observed in fluid planets. Souriau et al. (2003) studied polar caps using S3KS-S2KS body waves. No difference between the north and south caps were found, but most importantly no polar caps appear different from the mean earth, no heterogeneity related to a stagnant material can be detected (Souriau et al. (2003)). Which is again an argument against the polar cap theory.

The fact that the "L-shape" is not as perfect as observed for the cylinder differential times, might be caused by uneven sampling and/or by the fact that the cylinder might have a more complex structure than assumed. The dynamics of the tangent cylinder model indicates that the cylinder is surrounded by irregular vorteces, therefore the detailed shape of the distinct region, might not be perfectly cylindrical. Convection is limited to the region outside the tangent cylinder. Olson et al. (1999) suggested that elongated individual vorteces surround the tangent cylinder and inside the cylinder conditions are sub-critical for convection and the motion there is weak. A complication with these studies of outer core structures is the validity to sustain density heterogeneities in a turbulent convecting outer core, which consists of a low viscosity fluid (~10^{-4} Pa.s, comparable to water). Heterogeneities in the liquid outer core have generally been refused (Stevenson (1987); Souriau et al. (2003)). To resolve this, the tangent cylinder can only form if anisotropy is requested, since then no density heterogeneity is needed. (Souriau et al. (2003)). Anisotropy in the outer core might sustain and it is due to the circulation within the tangent cylinder that the cylinder is isolated from the convection outside the cylinder. Conceptually, it can be possible that light elements, dissipated during crystallization of the inner core, might concentrate inside vortices in and around the tangent cylinder, causing a velocity increase inside this region. If the increase in concentration of lighter elements will be maintained by the actual balance of forces within the outer core, still needs to be determined (Romanowicz et al. (2003)). Also, anisotropy in the outer core is not observed by Souriau et al. (2003), who studied outer core anisotropy and it is questionable whether anisotropy could be present in a liquid instead of a solid.

Conclusions

We find here both the tangent cylinder model in the outer core, proposed by Romanowicz and Bréger (2000), as well as inner core anisotropy (Morelli et al. (1986)) are able to explain observed PKPbc-PKPdf and PKPab-PKPdf differential travel times. Nevertheless, the low physical plausibility of the tangent cylinder and the smaller misfit of the inner core anisotropy model, favor inner core anisotropy. However, since the velocities within the cylinder are realistic and the misfit is relatively low, seismologically, the tangent cylinder model cannot be ruled out and needs further consideration. The polar cap models show unrealistic velocity increases and fit the data poorly, therefore the polar cap theory does not need to be pursued further. More research is necessary to find if there is a trade-off needed between outer core structures and inner core anisotropy, or one of the two models.

Even though no hemispheres have been used in my models, the paths are such that it seems that there are hemispherical difference. This means that we should be careful with interpreting hemispherical differences in the PKP travel time data as an isotropic eastern hemisphere and an anisotropic western hemisphere in the inner core.

Appendix A

PKIKP and PKPab/bc polar caps depths

I wrote a Fortran program 'polarcaps.f90' that determines for all PKIKP, PKPbc and PKPab waves of both datasets the depths in km's from where the waves pass the polar caps. The phi value and latitudes (indicated in blue) can be changed for different cap sizes. The phi is the angle between the cap boundary latitude (here (-)60°) and the north/south pole ((-)90°). One of the 'if-then-else'-statements can be excluded when running separate north and south cap models.

```
program polarcaps
implicit none

integer n,i,j,oucap,incap
real radius_outercore,theta,x,y,pi,phi,rad,radtheta,maxradius
real radius(745),gcarc(745),lat(745),lon(745)

radius_outercore=3471.
n=745
phi=30
pi = 4.*atan(1.)
rad=(pi/180.)*phi
x=radius_outercore*(cos(rad))
open(unit=124,file='depths_cap.dat',action='write',status='replace')
read(*,*)

   do i=1,n
read(*,*) gcarc(i),radius(i),lat(i),lon(i)
if (radius(i)<radius_outercore) then
incap=6371.-radius(i)
if (lat(i)<-60.)then
theta=(-90)-lat(i)
```

```
radtheta=(pi/180.)*theta
y=x/(cos(radtheta))
oucap=6371.-y
print *, incap,oucap
write(124,*) incap,oucap
else if (lat(i)>60.)then
theta=(90)-lat(i)
radtheta=(pi/180.)*theta
y=x/(cos(radtheta))
oucap=6371.-y
print *, incap,oucap
write(124,*) incap,oucap
else
incap=0.
oucap=0.
print *, incap,oucap
write(124,*) incap,oucap
end if
exit
end if
end do

do j=1,n
read(*,*) gcarc(j),radius(j),lat(j),lon(j)
if (radius(j)>radius_outercore) then
oucap=6371.-radius(j-1)
if (lat(j-1)<-60.)then
theta=(-90)-lat(j-1)
radtheta=(pi/180.)*theta
y=x/(cos(radtheta))
incap=6371.-y
print *, incap,oucap
write(124,*) incap,oucap
else if (lat(j-1)>60.)then
theta=(90)-lat(j-1)
radtheta=(pi/180.)*theta
y=x/(cos(radtheta))
incap=6371.-y
print *, incap,oucap
```

```
write(124,*) incap,oucap
else
incap=0.
oucap=0.
write(124,*) incap,oucap
print *, incap,oucap
end if
exit
end if
end do
close(unit=124)
stop


end program
```

Appendix B

Tangent cylinder depths for PKIKP waves

I wrote the Fortran program 'tangentcylinderPKIKP.f90' to determine the depths of where the PKIKP waves of both datasets are calculated. *'incyl1'* is the depth where the PKIKP wave first enters the cylinder before its turning point, *'oucyl1'* is the depth of the PKIKP where it leaves the tangent cylinder before its turning point-depth has been reached, *'incyl2'* is the depth where the PKIKP wave enters the tangent cylinder after it has reached its turning point and left the outer core, and lastly, *'oucyl2'* is the depth where the PKIKP leaves the tangent cylinder after is has reached its turning point (see below).

```
program tangentcylinderPKIKP
implicit none
integer n,i,j,k,l,incyl1,oucyl1,incyl2,oucyl2
real radius_outercore,theta,x,y,pi,phi,radtheta,oucap,maxradius,depth
real radius_innercore
real radius(777),gcarc(777),lat(777),lon(777),distance(777),rad(777)
radius_outercore=3471.
n=777
phi=30
pi = 4.*atan(1.)
radius_innercore=1250.
open(unit=124,file='depths_tangent.dat',action='write',status='replace')
open(unit=123,file='path_cylPKIKP.dat.gmt',action='read',status='old')
read(123,*)

do i=1,n
read(123,*) gcarc(i),radius(i),lat(i),lon(i)
depth=6371.-radius(i)
rad(i)=(pi/180.)*(90-abs(lat(i)))
distance(i)=radius(i)*sin(rad(i))
if (distance(i)<radius_innercore .and.  radius(i)>radius_innercore .and.  &
```

```
radius(i)<radius_outercore) then
incyl1=6371.-radius(i)
print *, incyl1
write(124,*)incyl1
exit
elseif (distance(i)<radius_innercore .and.  radius(i)>radius_outercore) then
incyl1=6371.-radius_outercore
print *, incyl1
write(124,*)incyl1
exit
elseif (distance(i)<radius_innercore .and.  radius(i)<radius_innercore) then
incyl1=0
print *, incyl1
write(124,*)incyl1
exit
end if
end do

do k=1,n
read(123,*) gcarc(k),radius(k),lat(k),lon(k)
if (incyl1/=0 .and.  radius(k)<radius_innercore) then
oucyl1=6371.-radius(k-1)
print *, oucyl1
write(124,*)oucyl1
exit
elseif (incyl1 .eq.  0) then
oucyl1=0
print *, oucyl1
write(124,*)oucyl1
exit
end if
end do

do l=1,n
read(123,*) gcarc(l),radius(l),lat(l),lon(l)
rad(l)=(pi/180.)*(90-abs(lat(l)))
distance(l)=radius(l)*sin(rad(l))
if (radius(l)>radius_innercore .and.  distance(l)<radius_innercore) then
incyl2=6371.-radius(l)
```

```
print *, incyl2
write(124,*)incyl2
exit
elseif (radius(l)>radius_innercore .and.  distance(l)>radius_innercore) then
incyl2=0
print *, incyl2
write(124,*)incyl2
exit
end if
end do

do j=1,n
read(123,*) gcarc(j),radius(j),lat(j),lon(j)
rad(j)=(pi/180.)*(90-abs(lat(j)))
distance(j)=radius(j)*sin(rad(j))
if (incyl2.eq.0.)  then
oucyl2=0
print *, oucyl2
write(124,*)oucyl2
exit
elseif (incyl2/=0.  .and.  distance(j)>radius_innercore .and.  &
radius(j)<radius_outercore) then
oucyl2=6371.-radius(j-1)
print *, oucyl2
write(124,*)oucyl2
exit
elseif (incyl2/=0.  .and.  radius(j)>radius_outercore) then
oucyl2=6371.-radius_outercore
print *, oucyl2
write(124,*)oucyl2
exit
end if
end do
close(unit=123)
close(unit=124)
stop

end program
```

Appendix C

Tangent cylinder depths for PKPab and PKPbc waves

I wrote a Fortran program 'tangentcylinderPKP.f90' to determine the depths where the PKPab and PKPbc waves enter and leave the tangent cylinder. The depths: *'incyl1', 'oucyl1', 'incyl2'* and *'oucyl2'* have the same description as mentioned in appendix B.

```
program tangentcylinderPKP
implicit none
integer n,i,j,k,l,m,o,io,ios,iot,iop,p,iom,incyl1,incyl2
integer oucyl1,oucyl2,turadinteger,ou
real radius_outercore,theta,x,y,pi,phi,radtheta,oucap,maxradius,depth
real radius_innercore,quarter,raad,a,tudp,b,tula,tulo,turad,diff
real radius(679),gcarc(679),lat(679),lon(679),distance(679),rad(679)
real oldradius(697),newradius(679)
radius_outercore=3471.
n=679
p=n/2
phi=30
pi = 4.*atan(1.)
radius_innercore=1220.

open(unit=125,file='path_cylPKPab.dat.gmt',action='read',status='old')
read(125,*) !skip first line of file
read(125,*) gcarc(1),radius(1),lat(1),lon(1)
do o=1,n
read(125,*) gcarc(o),radius(o),lat(o),lon(o)
diff=radius(o)-radius(o-1)
if (diff .gt.  0 .and.  diff .lt.  5000) then
turad=radius(o-1)
exit
```

```
end if
end do
close(125)
open(unit=124,file='depths_tangentab.dat',action='write',status='replace')
open(unit=123,file='path_cylPKPab.dat.gmt',action='read',status='old')
read(123,*)

do i=1,n
read(123,*,IOSTAT=io) gcarc(i),radius(i),lat(i),lon(i)
if (radius(i).gt.turad) then
if (io .eq.  0) then
rad(i)=(pi/180.)*(90-abs(lat(i)))
distance(i)=radius(i)*sin(rad(i))
if (distance(i)<radius_innercore .and.  radius(i)<radius_outercore) then
incyl1=6371.-radius(i)
print *, incyl1
write(124,*)incyl1
exit
elseif (distance(i)<radius_innercore .and.  radius(i)>radius_outercore) then
incyl1=6371.-radius_outercore
print *, incyl1
write(124,*)incyl1
exit
end if
elseif (io .gt.  0) then
incyl1=6371
print *, incyl1
write(124,*)incyl1
exit
elseif (io .lt.  0) then
incyl1=6371
print *, incyl1
write(124,*)incyl1
exit
end if
elseif (radius(i) .eq.  turad) then
incyl1=1
print *, incyl1
write(124,*)incyl1
```

```
exit
end if
end do

if (incyl1.eq.0) then
print *, incyl1
write(124,*)incyl1
end if

do j=1,(n)
read(123,*,IOSTAT=ios) gcarc(j),radius(j),lat(j),lon(j)
if (radius(j).gt.turad) then
if (incyl1 /= 6371 .and.  ios .eq.  0 .and.  incyl1 /= 0 .and.  incyl1 /= 1)&
then
rad(j)=(pi/180.)*(90-abs(lat(j)))
distance(j)=radius(j)*sin(rad(j))
if (distance(j)>radius_innercore .and.  radius(j)<radius_outercore) then
oucyl1=6371.-radius(j-1)
print *, oucyl1
write(124,*)oucyl1
exit
elseif (distance(j)>radius_innercore .and.  radius(j)>radius_outercore) then
oucyl1=6371.-radius_outercore
print *, oucyl1
write(124,*)oucyl1
exit
end if
elseif (incyl1 .eq.  6371 .or.  ios .lt.  0 .or.  incyl1 .eq.  0) then
oucyl1=6371
print *, oucyl1
write(124,*)oucyl1
exit
elseif (incyl1 .eq.  6371 .or.  ios .gt.  0 .or.  incyl1 .eq.  1) then
oucyl1= 6371
print *, oucyl1
write(124,*)oucyl1
exit
end if
elseif (radius(j).eq.turad .and.  incyl1 /= 1) then
```

```
oucyl1=1
print *, oucyl1
write(124,*)oucyl1
exit
end if
end do

!=============================================================
do m=1,n/2
read(123,*,IOSTAT=iom) gcarc(m),radius(m),lat(m),lon(m)
if (radius(m).eq.turad .and.  iom.eq.0) then
exit
elseif (oucyl1 .eq.  1 ) then
rad(m)=(pi/180.)*(90-abs(lat(m)))
distance(m)=radius(m)*sin(rad(m))
if (distance(m)>radius_innercore .and.  radius(m)<radius_outercore) then
incyl2=6371.-radius(m-1)
print *, incyl2
write(124,*)incyl2
exit
elseif (distance(m)>radius_innercore .and.  radius(m)>radius_outercore) then
incyl2=6371.-radius_outercore
print *, incyl2
write(124,*)incyl2
exit
end if
elseif (incyl1 .eq.  1) then
rad(m)=(pi/180.)*(90-abs(lat(m)))
distance(m)=radius(m)*sin(rad(m))
if (distance(m)<radius_innercore .and.  radius(m)<radius_outercore) then
incyl2=6371.-radius(m)
print *, incyl2
write(124,*)incyl2
exit
elseif (distance(m)<radius_innercore .and.  radius(m)>radius_outercore) then
incyl2=6371.-radius_outercore
print *, incyl2
write(124,*) incyl2
exit
```

```
end if
end if
end do
!=========================================================

   do k=1,n
read(123,*,IOSTAT=iot) gcarc(k),radius(k),lat(k),lon(k)
if (iot .eq. 0 .and. incyl2/=6371 .and. incyl2.eq.0) then
rad(k)=(pi/180.)*(90-abs(lat(k)))
distance(k)=radius(k)*sin(rad(k))
if (distance(k)<radius_innercore .and. radius(k)<radius_outercore) then
incyl2=6371.-radius(k)
print *, incyl2
write(124,*)incyl2
exit
elseif (distance(k)<radius_innercore .and. radius(k)>radius_outercore) then
incyl2=6371.-radius_outercore
print *, incyl2
write(124,*)incyl2
exit
end if
elseif (iot .gt. 0 .and. incyl2/=6371 .and. oucyl1 /= 1) then
incyl2=6371
print *, incyl2
write(124,*)incyl2
exit
elseif (iot .lt. 0 .and. incyl2/=6371 .and. oucyl1 .ne. 1) then
incyl2=6371
print *, incyl2
write(124,*)incyl2
exit
elseif (oucyl1.eq. 1 .and. iot .lt. 0) then
oucyl2=6371
print *, oucyl2
write(124,*)oucyl2
exit
elseif (oucyl1.eq.1 .and. iot .gt. 0) then
oucyl2=6371
print *, oucyl2
```

```
write(124,*)oucyl2
exit
elseif (incyl1 .eq.  1) then
exit
end if
end do

do l=1,n read(123,*,IOSTAT=iop) gcarc(l),radius(l),lat(l),lon(l)
if (incyl2 /= 6371 .and.  iop .eq.  0 .and.  oucyl2 /= 6371 .and.  oucyl1/= 1)
then
rad(l)=(pi/180.)*(90-abs(lat(l)))
distance(l)=radius(l)*sin(rad(l))
if (distance(l)>radius_innercore .and.  radius(l)<radius_outercore) then
oucyl2=6371.-radius(l-1)
print *, oucyl2
write(124,*)oucyl2
exit
elseif (distance(l)>radius_innercore .and.  radius(l)>radius_outercore) then
oucyl2=6371.-radius_outercore
print *, oucyl2
write(124,*)oucyl2
exit
end if
elseif (incyl2 .eq.  6371 .and.  oucyl2 /= 6371 .and.  oucyl1/=1) then
oucyl2=6371
print *, oucyl2
write(124,*)oucyl2
exit
elseif (incyl2 .eq.  6371 .or.  iop .gt.  0 .and.  oucyl2 /= 6371 .and.  oucyl1/=1)
then
oucyl2=6371
print *, oucyl2
write(124,*)oucyl2
exit
elseif (ios .lt.  0) then
oucyl2=0
print *, oucyl2
exit
end if
```

```
end do

close(123)
close(124)
stop

end program
```

Appendix D

Depths in cylinder and arrival times PKIKP waves

In this appendix the depths of the PKIKP waves entering the tangent cylinder in the outer core and its corresponding arrival times, calculated by TauP, are shown from the 2008-04-14 event at the South Sandwich Islands region. The same has been done for PKPab waves and, thereafter, the difference between both total cylinder times gives the cylinder differential times shown in the plots. The same methods is applied for the polar caps model. Number one depth gives the depth the PKIKP wave entering the tangent cylinder before passing the inner core ('incyl1'). Number two depth is the depth leaving the tangent cylinder; with 5103 km as the inner-outer core boundary ('oucyl1'). Number three depth is the depth entering the tangent cylinder after passing the inner core; with again 5103km as the inner-outer core boundary ('incyl2') and finally the number four depth is the depth when the PKIKP wave leaves the tangent cylinder after passing the inner core ('oucyl2'). The 'incyl1time' is the time spend in the tangent cylinder before the wave has passed the inner core and the 'incyl2time' is the time spend in the tangent cylinder after passing the inner core. These numbers added gives the total amount of time the PKIKP wave spends in the tangent cylinder.

1) 3869 km 2) 5103 km 3) 5103 km 4) 5083 km intime_incyl1PKIKP= 357.9 intime_oucyl1PKIKP= 496.2 outtime_incyl2PKIKP= 664.7 outtime_oucyl2PKIKP= 667.1 icyl1time_PKIKP= 138.3 icyl2time_PKIKP= 2.4 totaltimecylinder_PKIKP= **140.7**

1) 3882 km 2) 5103 km 3) 5103 km 4) 5083 km intime_incyl1PKIKP= 359.3 intime_oucyl1PKIKP= 496.0 outtime_incyl2PKIKP= 665.0 outtime_oucyl2PKIKP= 667.4 icyl1time_PKIKP= 136.7 icyl2time_PKIKP= 2.4 totaltimecylinder_PKIKP= **139.1**

1) 3950 km 2) 5103 km 3) 5103 km 4) 5053 km intime_incyl1PKIKP= 366.7 intime_oucyl1PKIKP= 495.7 outtime_incyl2PKIKP= 665.5 outtime_oucyl2PKIKP= 671.6 icyl1time_PKIKP= 129 icyl2time_PKIKP= 6.1 totaltimecylinder_PKIKP= **135.1**

1) 3953 km 2) 5103 km 3) 5103 km 4) 5053 km intime_incyl1PKIKP= 367.1 intime_oucyl1PKIKP= 495.7 outtime_incyl2PKIKP= 665.5 outtime_oucyl2PKIKP= 671.6 icyl1time_PKIKP= 128.6 icyl2time_PKIKP= 6.1 totaltimecylinder_PKIKP= **134.7**

1) 3959 km 2) 5103 km 3) 5103 km 4) 5053 km intime_incyl1PKIKP= 367.7 intime_oucyl1PKIKP= 495.7 outtime_incyl2PKIKP= 665.5 outtime_oucyl2PKIKP= 671.6 icyl1time_PKIKP= 128 icyl2time_PKIKP= 6.1 totaltimecylinder_PKIKP= **134.1**

1) 4147 km 2) 5103 km 3) 5103 km 4) 4977 km intime_incyl1PKIKP= 388.6 intime_oucyl1PKIKP= 496.1 outtime_incyl2PKIKP= 664.7 outtime_oucyl2PKIKP= 679.8 icyl1time_PKIKP= 107.5 icyl2time_PKIKP= 15.1 totaltimecylinder_PKIKP= **122.6**

1) 4147 km 2) 5103 km 3) 5103 km 4) 4977 km intime_incyl1PKIKP= 388.6 intime_oucyl1PKIKP= 496.2 outtime_incyl2PKIKP= 664.6 outtime_oucyl2PKIKP= 679.8 icyl1time_PKIKP= 107.6 icyl2time_PKIKP= 15.2 totaltimecylinder_PKIKP= **122.8**

1) 4298 km 2) 5103 km 3) 5103 km 4) 4700 km intime_incyl1PKIKP= 402.1 intime_oucyl1PKIKP= 489.4 outtime_incyl2PKIKP= 676.5 outtime_oucyl2PKIKP= 720.8 icyl1time_PKIKP= 87.3 icyl2time_PKIKP= 44.3 totaltimecylinder_PKIKP= **131.6**

1) 4499 km 2) 5103 km 3) 5103 km 4) 4650 km intime_incyl1PKIKP= 426.9 intime_oucyl1PKIKP= 495.7 outtime_incyl2PKIKP= 665.4 outtime_oucyl2PKIKP= 717.6 icyl1time_PKIKP= 68.8 icyl2time_PKIKP= 52.2 totaltimecylinder_PKIKP= **121**

1) 4600 km 2) 5103 km 3) 5103 km 4) 2900 km intime_incyl1PKIKP= 429.7 intime_oucyl1PKIKP= 481.6 outtime_incyl2PKIKP= 690.3 outtime_oucyl2PKIKP= 931.0 icyl1time_PKIKP= 51.9 icyl2time_PKIKP= 240.7 totaltimecylinder_PKIKP= **292.6**

1) 3597 km 2) 5103 km 3) 5103 km 4) 6371 km intime_incyl1PKIKP= 326.2 intime_oucyl1PKIKP= 491.9 outtime_incyl2PKIKP= 672.2 outtime_oucyl2PKIKP= 672.2 icyl1time_PKIKP= 165.7 icyl2time_PKIKP= 0 totaltimecylinder_PKIKP= **165.7**

1) 3597 km 2) 5103 km 3) 5103 km 4) 6371 km intime_incyl1PKIKP= 326.2 intime_oucyl1PKIKP= 491.9 outtime_incyl2PKIKP= 672.2 outtime_oucyl2PKIKP= 672.2 icyl1time_PKIKP= 165.7 icyl2time_PKIKP= 0 totaltimecylinder_PKIKP= **165.7**

1) 4427 km 2) 5103 km 3) 5103 km 4) 3629 km intime_incyl1PKIKP= 411.3 intime_oucyl1PKIKP= 480.8 outtime_incyl2PKIKP= 691.9 outtime_oucyl2PKIKP= 846.3 icyl1time_PKIKP= 69.5 icyl2time_PKIKP= 154.4 totaltimecylinder_PKIKP= **223.9**

1) 3869 km 2) 5103 km 3) 5103 km 4) 4801 km intime_incyl1PKIKP= 351.9 intime_oucyl1PKIKP= 479.0 outtime_incyl2PKIKP= 695.1 outtime_oucyl2PKIKP= 725.6 icyl1time_PKIKP= 127.1 icyl2time_PKIKP=

30.5 totaltimecylinder_PKIKP= **157.6**

1) 3895 km 2) 5103 km 3) 5103 km 4) 5083 km intime_incyl1PKIKP= 361.0 intime_oucyl1PKIKP= 496.7 outtime_incyl2PKIKP= 663.6 outtime_oucyl2PKIKP= 666.1 icyl1time_PKIKP= 135.7 icyl2time_PKIKP= 2.5 totaltimecylinder_PKIKP= **138.2**

1) 3895 km 2) 5103 km 3) 5103 km 4) 5083 km intime_incyl1PKIKP= 360.9 intime_oucyl1PKIKP= 496.4 outtime_incyl2PKIKP= 664.2 outtime_oucyl2PKIKP= 666.6 icyl1time_PKIKP= 135.5 icyl2time_PKIKP= 2.4 totaltimecylinder_PKIKP= **137.9**

1) 3895 km 2) 5103 km 3) 5103 km 4) 5083 km intime_incyl1PKIKP= 360.9 intime_oucyl1PKIKP= 496.4 outtime_incyl2PKIKP= 664.2 outtime_oucyl2PKIKP= 666.6 icyl1time_PKIKP= 135.5 icyl2time_PKIKP= 2.4 totaltimecylinder_PKIKP= **137.9**

Bibliography

Beghein, C. and Trampert, J. (2003). Robust normal mode constraints on inner-core anisotropy from model space search. *Science*, 299(5606):552–555.

Bréger, L., Romanowicz, B., and Tkalčić, H. (1999). Pkp (bc-df) travel time residuals and short scale heterogeneity in the deep earth. *Geophysical research letters*, 26(20):3169–3172.

Bréger, L., Tkalčić, H., and Romanowicz, B. (2000). The effect of d on pkp (ab- df) travel time residuals and possible implications for inner core structure. *Earth and Planetary Science Letters*, 175(1):133–143.

Creager, K. C. (1999). Large-scale variations in inner core anisotropy. *Journal of Geophysical Research: Solid Earth*, 104(B10):23127–23139.

Deuss, A. (2014). Heterogeneity and anisotropy of earth's inner core. *Annual Review of Earth and Planetary Sciences*, 42:103–126.

Deuss, A., Irving, J. C., and Woodhouse, J. H. (2010). Regional variation of inner core anisotropy from seismic normal mode observations. *Science*, 328(5981):1018–1020.

Dziewonski, A., Chou, T.-A., and Woodhouse, J. (1981). Determination of earthquake source parameters from waveform data for studies of global and regional seismicity. *Journal of Geophysical Research: Solid Earth*, 86(B4):2825–2852.

Ekström, G., Nettles, M., and Dziewoński, A. (2012). The global cmt project 2004–2010: centroid-moment tensors for 13,017 earthquakes. *Physics of the Earth and Planetary Interiors*, 200:1–9.

Engdahl, E. R., van der Hilst, R., and Buland, R. (1998). Global teleseismic earthquake relocation with improved travel times and procedures for depth determination. *Bulletin of the Seismological Society of America*, 88(3):722–743.

Hrvoje, T., Barbara, R., and Nicolas, H. (2002). Constraints on d structure using pkp (ab–df), pkp (bc–df) and pcp–p traveltime data from broad-band records. *Geophysical Journal International*, 149(3):599–616.

Hulot, G., Eymin, C., Langlais, B., Mandea, M., and Olsen, N. (2002). Small-scale structure of the geodynamo inferred from oersted and magsat satellite data. *Nature*, 416(6881):620–623.

Irving, J. and Deuss, A. (2011). Hemispherical structure in inner core velocity anisotropy. *Journal of Geophysical Research: Solid Earth*, 116(B4).

Ishii, M. and Dziewoński, A. M. (2002). The innermost inner core of the earth: Evidence for a change in anisotropic behavior at the radius of about 300 km. *Proceedings of the National Academy of Sciences*, 99(22):14026–14030.

Ishii, M., Tromp, J., Dziewoński, A. M., and Ekström, G. (2002). Joint inversion of normal mode and body wave data for inner core anisotropy 1. laterally homogeneous anisotropy. *Journal of Geophysical Research: Solid Earth*, 107(B12).

Kennett, B., Engdahl, E., and Buland, R. (1995). Constraints on seismic velocities in the earth from traveltimes. *Geophysical Journal International*, 122(1):108–124.

Lehmann, I. (1936). P: Publications du bureau central séismologique international. *A14*, pages 87–115.

Morelli, A., Dziewonski, A. M., and Woodhouse, J. H. (1986). Anisotropy of the inner core inferred from pkikp travel times. *Geophysical Research Letters*, 13(13):1545–1548.

Oldham, R. D. (1906). The constitution of the interior of the earth, as revealed by earthquakes. *Quarterly Journal of the Geological Society*, 62(1-4):456–475.

Olson, P., Christensen, U., and Glatzmaier, G. A. (1999). Numerical modeling of the geodynamo: mechanisms of field generation and equilibration. *Journal of Geophysical Research: Solid Earth*, 104(B5):10383–10404.

Poupinet, G., Pillet, R., and Souriau, A. (1983). Possible heterogeneity of the earth's core deduced from pkikp travel times. *Nature*, 305(5931):204–206.

Ritzwoller, M., Masters, G., and Gilbert, F. (1986). Observations of anomalous splitting and their interpretation in terms of aspherical structure. *Journal of Geophysical Research: Solid Earth*, 91(B10):10203–10228.

Romanowicz, B. and Bréger, L. (2000). Anomalous splitting of free oscillations: a reevaluation of possible interpretations. *Journal of Geophysical Research: Solid Earth*, 105(B9):21559–21578.

Romanowicz, B., TkalčIč, H., and Breger, L. (2003). On the origin of complexity in pkp travel time data. *Earth's Core: Dynamics, Structure, Rotation*, pages 31–44.

Shearer, P. M., Toy, K. M., and Orcutt, J. A. (1988). Axi-symmetric earth models and inner-core anisotropy. *Nature*, 333(6170):228–232.

Song, X. and Helmberger, D. V. (1998). Seismic evidence for an inner core transition zone. *Science*, 282(5390):924–927.

Souriau, A. and Poupinet, G. (1990). A latitudinal pattern in the structure of the outermost liquid core, revealed by the travel times of skks-sks seismic phases. *Geophysical Research Letters*, 17(11):2005–2007.

Souriau, A., Teste, A., and Chevrot, S. (2003). Is there any structure inside the liquid outer core? *Geophysical research letters*, 30(11).

Stevenson, D. (1987). Limits on lateral density and velocity variations in the earth's outer core. *Geophysical Journal International*, 88(1):311–319.

Stixrude, L. and Cohen, R. (1995). High-pressure elasticity of iron and anisotropy of earth's inner core. *Science*, 267(5206):1972.

Su, W.-j. and Dziewonski, A. M. (1995). Inner core anisotropy in three dimensions. *Journal of Geophysical Research: Solid Earth*, 100(B6):9831–9852.

Tanaka, S. and Hamaguchi, H. (1997). Degree one heterogeneity and hemispherical variation of anisotropy in the inner core from pkp (bc)–pkp (df) times. *Journal of Geophysical Research: Solid Earth*, 102(B2):2925–2938.

Woodhouse, J. H., Giardini, D., and Li, X.-D. (1986). Evidence for inner core anisotropy from free oscillations. *Geophysical Research Letters*, 13(13):1549–1552.